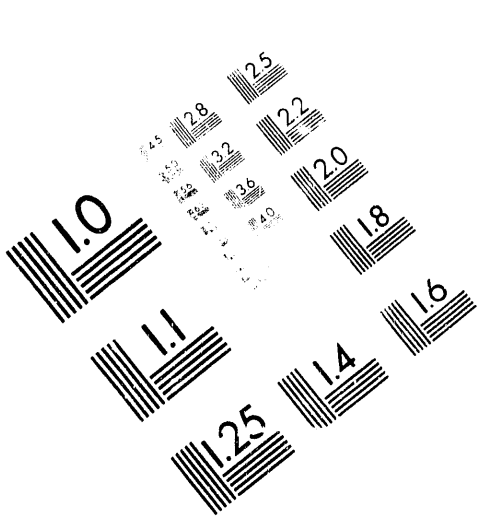

Association for Information and Image Management
1100 Wayne Avenue, Suite 1100
Silver Spring, Maryland 20910
301/587-8202

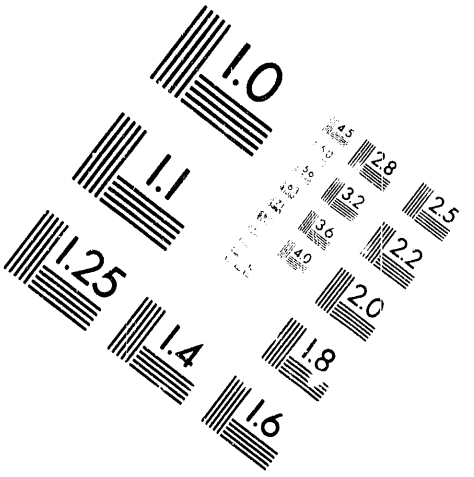

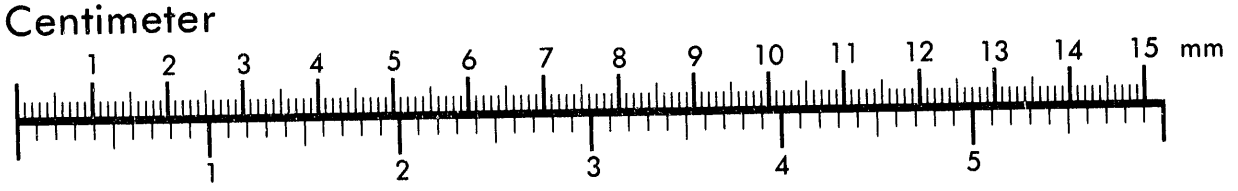

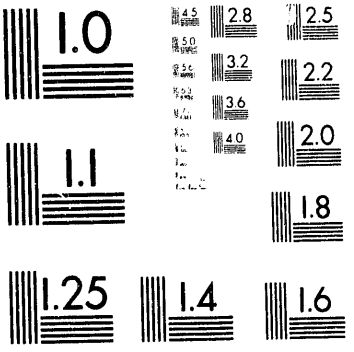

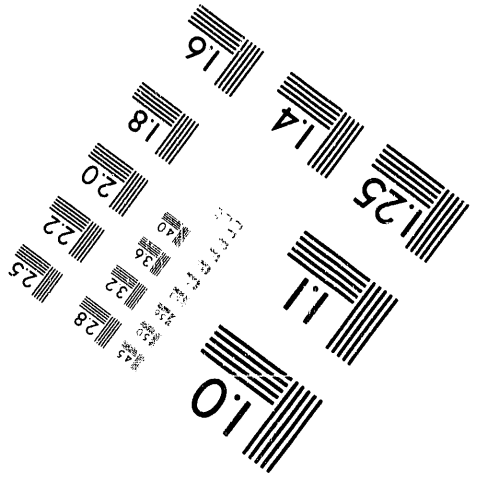

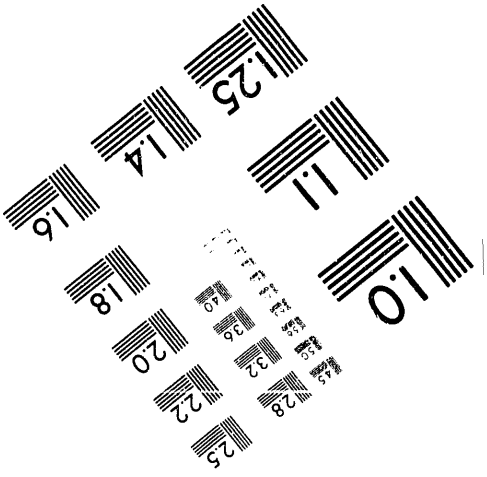

1 of 1

Distribution Category:
Fuel Cells
(UC-110)

ANL-92/24

ANL--92/24

DE93 008900

Argonne National Laboratory
9700 South Cass Avenue,
Argonne, Illinois 60439

NONDESTRUCTIVE CHARACTERIZATION METHODS FOR MONOLITHIC SOLID OXIDE FUEL CELLS

by

William A. Ellingson

Electrochemical Technology Program
and
Materials and Components Technology Division

January 1993

Work sponsored by

U.S. Department of Energy
Office of Fossil Energy
Morgantown Energy Technology Center

CONTENTS

FIGURES

TABLES

NONDESTRUCTIVE CHARACTERIZATION METHODS FOR MONOLITHIC SOLID OXIDE FUEL CELLS

by

William A. Ellingson

ABSTRACT

Monolithic solid oxide fuel cells (MSOFCs) represent a potential breakthrough in fuel cell technology, provided that reliable fabrication methods can be developed. Fabrication difficulties arise in several steps of the processing: *First* is the fabrication of uniform thin (305 μm) single-layer and trilayer green tapes (the trilayer tapes of anode/electrolyte/cathode and anode/interconnect/cathode must have similar coefficients of thermal expansion to sinter uniformly and to have the necessary electrochemical properties); *Second* is the development of fuel and oxidant channels in which residual stresses are likely to develop in the tapes; *Third* is the fabrication of a "complete" cell for which the bond quality between layers and the quality of the trilayers must be established; and *Last*, attachment of fuel and oxidant manifolds and verification of seal integrity.

The purpose of this report is to assess nondestructive characterization methods that could be developed for application to laboratory, prototype, and full-scale MSOFCs.

1 INTRODUCTION

Solid oxide fuel cells are under development for many widely varying electric power generation applications,[1–3] including central electric power stations, transportation, and space-based uses. Fuel sources may vary but the two predominant fuels are hydrogen and oxygen.[4] The monolithic solid oxide fuel cell (MOSFC) is an advanced design concept that places thin (<100–300 μm) ceramic components in a lightweight, compact structure that uses the fuel and oxidant channels as part of its structure. Figure 1 shows schematically two MSOFC designs: a crossflow design in which the fuel and oxidant flows are in different layers, and a coflow design in which the fuel and oxidant flow in the same layer but in different channels. Two key features of the MSOFC design are its self-supporting structure and its high energy density (i.e., small cell size). For one design, a 25-kVe "stack"

of a crossflow design is only 37.5 x 37.5 x 34.4 cm high (14.75 x 14.75 x 13.5 in. high). The small size of the individual cells in the MSOFC minimizes voltage losses due to internal resistance, resulting in high efficiency and improved perfo. nance.

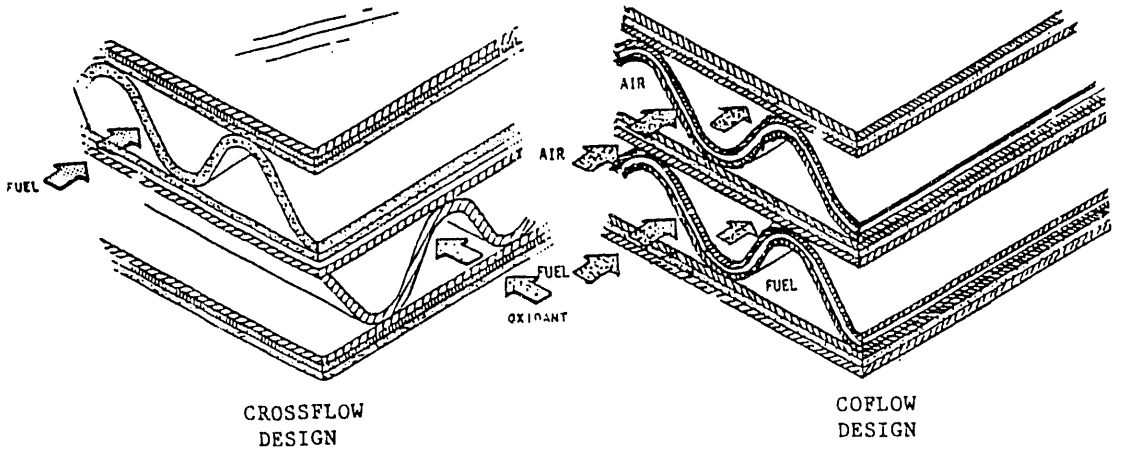

Fig. 1. Schematic diagram of flow-channel arrangements in a monolithic solid oxide fuel cell

In this report, the processing of an MSOFC has been studied and observations have been made on how nondestructive characterization might be applied at each process step. To better understand why certain nondestructive characterization methods are selected, it is important to understand the basic operating principle of a fuel cell and its fabrication process. These descriptions are followed by an interrelated discussion of processing and the nondestructive characterization methods selected for each process stage.

2 BACKGROUND OF MONOLITHIC SOLID OXIDE FUEL CELLS

The MSOFC design was first proposed by Argonne National Laboratory in 1983.

Basic Operating Principles

In an MSOFC that operates at 1000°C, fuel and oxidant produce direct current by combining electrochemically across a solid oxide electrolyte. Oxygen in the oxidant flowing through the cathode accepts electrons from the incoming circuit to form oxygen ions. The oxygen ions are conducted

through the dense electrolyte to the anode. At the anode, oxygen ions combine with hydrogen to form water vapor and liberate electrons, as shown in Fig. 2. Cells of an MSOFC are connected in series by a ceramic interconnect to build up the voltage. The interconnect carries electrons from the anode of one cell to the cathode of the next in electrical series.

In the coflow design, the MSOFC consists of a honeycomb-like array of adjacent fuel and oxidant channels that resemble ordinary corrugated paperboard (Fig. 3). Oxidant channels are lined with a porous cathode, and fuel channels are lined with a porous anode. A fully dense electrolyte is located between the anode and cathode. An interconnect, which is also fully dense, links the cells in electrical series. As can be seen in Fig. 3, the MSOFC is made of two types of laminated structures, each composed of three different ceramic compositions—anode/electrolyte/cathode (A/E/C) and anode/interconnect/cathode (A/I/C). The corrugations form gas seals at the edges of the monolithic structure.

In the crossflow design, fuel and oxidant channels are formed by the corrugated anode and cathode layers that are oriented at right angles to each other (Fig. 4).

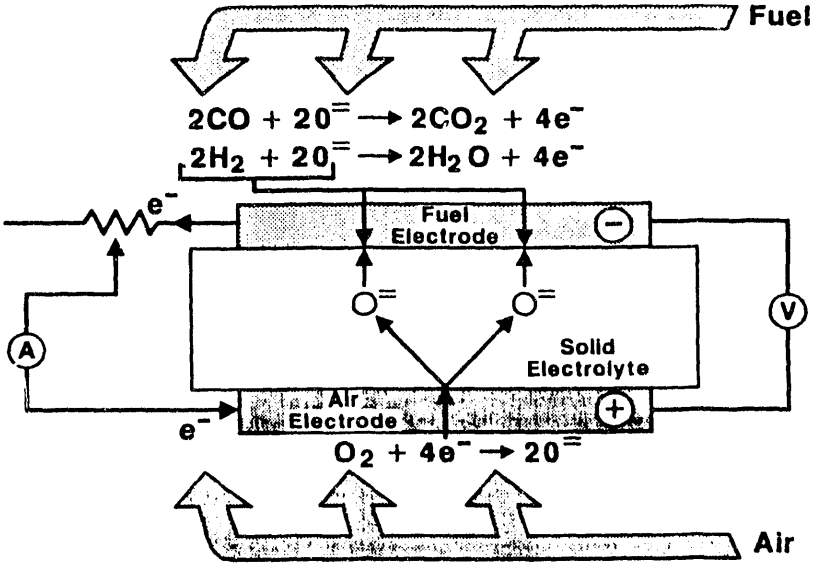

Fig. 2. Operating principle of the monolithic solid oxide fuel cell. (Figure courtesy of Gas Research Inst., Chicago, IL.)

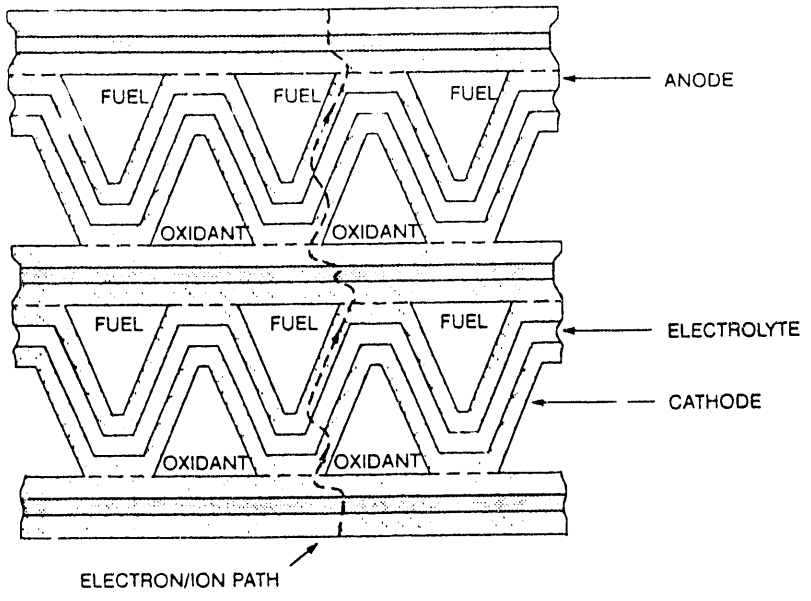

Fig. 3. Schematic diagram of coflow monolithic solid oxide fuel cell

The A/E/C and A/I/C composites are flat and stacked alternately between fuel and oxidant channels. The crossflow design results in a reduction in power density by a factor of about 2 relative to the coflow design; however, the crossflow design also offers simpler ducting of fuel and oxidant (manifolding). Because of this, the crossflow design is being developed first and is the focus of this report.

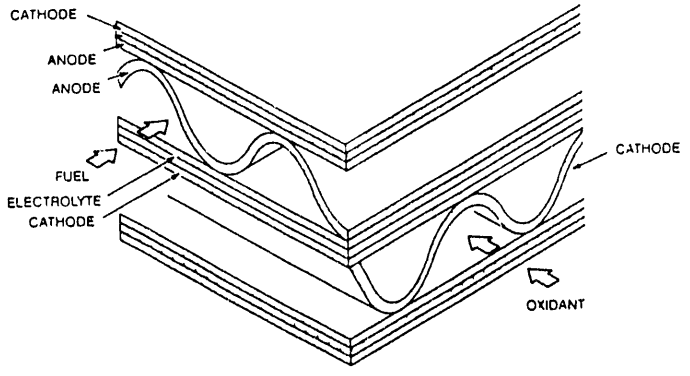

Fig. 4. Schematic diagram of crossflow monolithic solid oxide fuel cell

Composition and Properties of Individual Components

Each component is significantly different in chemical composition and in required properties. These are briefly discussed below and are summarized in Table 1.

- *Electrolyte (yttria-stabilized zirconia)*: Yttria-stabilized zirconia (YSZ) is the preferred solid electrolyte in most solid oxide fuel cells. The required properties of the electrolyte are high ionic conductivity, no gas leakage, high mechanical strength, and chemical compatibility with electrode materials and reaction gases.

- *Cathode (strontium-doped lanthanum manganite)*: At present, Sr-doped $LaMnO_3$ (10 mol% Sr) is used as the MSOFC cathode material. The electrical resistivity of Sr-doped $LaMnO_3$ at 1000°C (e.g., 84 ohm^{-1}–cm^{-1} at 75% density) exceeds the requirement for MSOFC cathodes (see Table 1).

  Strontium doping enhances the electronic conductivity of $LaMnO_3$. The thermal expansion coefficient of the material is about 11.5 x $10^{-6}°C^{-1}$ (room temperature to 1000°C), closely matching that of zirconia. One concern about $LaMnO_3$ as the cathode material for the MSOFC is manganese migration during processing and operation. Manganese is a very mobile species and can easily diffuse into the electrolyte in the range of the sintering temperature for the MSOFC.

- *Anode (nickel/zirconia cermet)*: Due to the reducing atmosphere of the fuel gas, metals can be used as electrode materials for the MSOFC anode. Nickel has been found to be particularly suitable. The functions of the zirconia in the MSOFC anode are to

  (a) Support the metallic nickel particles.

  (b) Inhibit coarsening of the metallic particles at the fuel cell operating temperature.

  (c) Provide an anode thermal expansion coefficient acceptably close to those of the other cell components.

Table 1. Material requirements for monolithic solid oxide fuel cells

Component	Resistivity	Stability	Compatibility	Porosity	Thermal Expansion	Firing Shrinkage	Other
Electrolyte	Ionic conductivity >0.03 ohm^{-1}–cm^{-1} at 1000°C Negligible electronic conductivity	Chemical stability in fuel and air environments	No damaging chemical interactions or interdiffusion with adjoining cell components	>94% dense	Thermal expansion must match adjoining cell components (about 11 x 10^{-6} cm/cm/°C, room temperature to 1000°C)	Linear shrinkage during firing must match other cell components Shrinkage should be as low as possible	Low gas permeability
Cathode	Electronic conductivity >50 ohm^{-1}–cm^{-1} at 1000°C	Chemical stability in air environment	No damaging chemical interactions or interdiffusion with adjoining cell components	About 20 to 50% porosity	Thermal expansion must match adjoining cell components (about 11 x 10^{-6} cm/cm/°C, room temperature to 1000°C)	Linear shrinkage during firing must match other cell components Shrinkage should be as low as possible	
Anode	Electronic conductivity >120 ohm^{-1}–cm^{-1} at 1000°C	Chemical stability in fuel environment	No damaging chemical interactions or interdiffusion with adjoining cell components	About 20 to 50% porosity	Thermal expansion must match adjoining cell components (about 11 x 10^{-6} cm/cm/°C, room temperature to 1000°C)	Linear shrinkage during firing must match other cell components Shrinkage should be as low as possible	Tolerance to sulfur contamination Sufficient catalytic activity for steam reforming of hydrocarbons

One concern with the nickel/zirconia cermet anode in the MSOFC is the high thermal expansion coefficient relative to the anode, interconnect, and electrolyte.

- *Interconnect (doped lanthanum chromite)*: The electronic conductivity of doped $LaCrO_3$ depends on the partial pressure of oxygen. The resistivity of the material exposed to fuel on one side and to oxidant on the other is about 5 ohm^{-1}-cm^{-1} at 1000°C.

The coefficients of thermal expansion have been found to be in the range of 8 x 10^{-6} to 11 x 10^{-6} $°C^{-1}$, depending on the type and amount of dopant present. For strontium-doped materials, it is about 10.7 x 10^{-6} $°C^{-1}$ (room temperature to 1000°C). Thus, the thermal expansion properties of Sr-doped $LaCrO_3$ are similar to those of ZrO_2.

$LaCrO_3$ is very difficult to densify under ambient atmospheric conditions. The sintering of $LaCrO_3$ to high densities requires firing temperatures greater than 1600°C under low oxygen partial pressures. Sintering aids have been used to improve the sinterability of $LaCrO_3$.

Fabrication

Discussion of Hot-Rolled Calendering and Corrugation Processes

The reliability of each fabrication step dominates the viability of the MSOFC. MSOFC stacks must be fabricated reproducibly without defects. Different defect types, however, can be introduced at each step of the fabrication process. In addition, current laboratory-scale fabrication processes must be viewed with an eye toward scale-up to commercialization.

As noted earlier, a major technical challenge in developing the MSOFC involves several details in fabricating the monolithic structure from special thin (<100-300 μm) ceramic single layers or trilayers.[5] Fabrication of the MSOFC requires many steps, including powder characterization, blending of powders and additives, forming thin ceramic component layers as green (unfired) bodies, laminating green tapes into trilayer composites, forming the fuel and oxidant channels in the green tapes, sintering the structure at elevated temperatures to form the requisite integral monolithic structure, and applying proper manifolding for transport of fuel and oxidant.

The fabrication methodology being developed for the MSOFC is hot-rolled calendering.[6,7] One of the advantages of this technique is its ability to handle the large-quantity and large-scale production anticipated for commercial scale-up conditions. Calendering can produce thin, uniform, strong and flexible single or multilayer tapes.[8–10] Initial work conducted at the AiResearch Los Angeles Division (ALAD) of Allied-Signal has demonstrated the suitability of the calendering technique for fabricating MSOFCs.

The fabrication scheme for the MSOFC based on the calendering technique is shown in Fig. 5. Ceramic powders, binders, and plasticizers are first blended in a mill and then mixed in a second blending mixer. The material plasticizes due to heat of friction during mixing and forms a plastic-like mass that is then calendered into a thin flat tape by a two-roll mill.

The calendering method uses two counterrotating chromium-coated stainless steel rollers with independent variable speed control. The temperature of the two rollers is regulated by independently controlled, circulating oil baths, and the separation between the rollers is adjustable to allow tape thickness to be controlled.

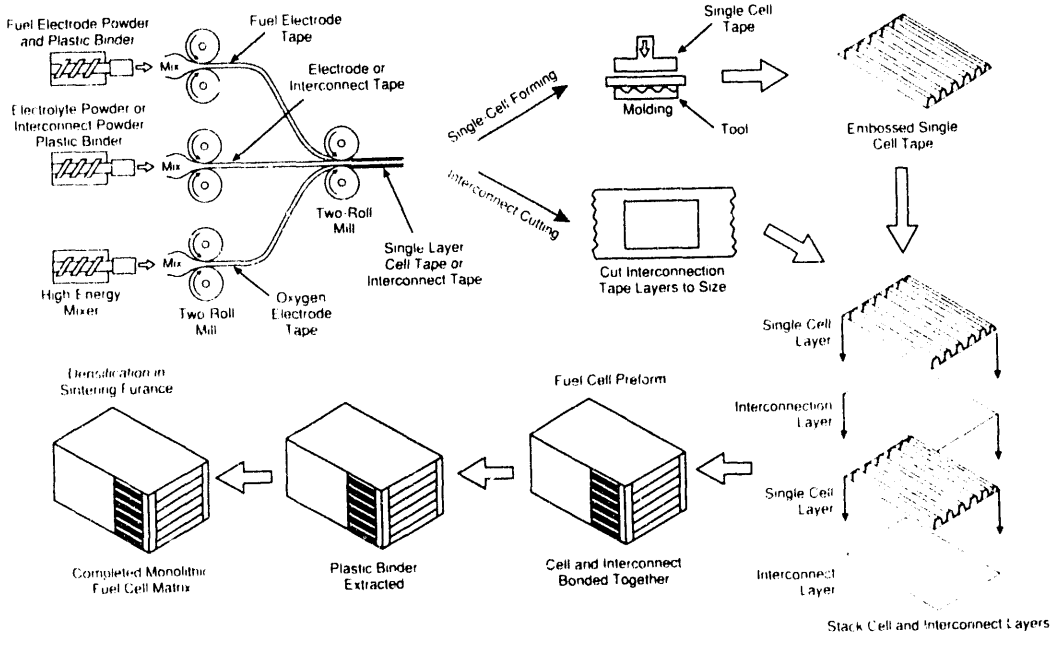

Fig. 5. Fabrication scheme based on calendering (Figure courtesy of Allied-Signal Aerospace Co., AiResearch Los Angeles Division.)

Individual tapes are laminated together in a second rolling operation to form trilayer tapes. The mechanical force in the second rolling operation bonds the layers. Figure 6 shows a cross section of a green trilayer composite fabricated by calendering.

To form the fuel and oxidant channels, single-layer tapes (305 μm thick) are corrugated. The corrugation method is based on a compression molding technique. A mold that is currently used to make corrugations in single-layer tapes is shown in Fig. 7. The mold is made in top and bottom halves, the top of rubber and the bottom half of aluminum. During fabrication, the bottom half of the mold is placed on a temperature-controlled hot plate. A piece of the hot-calendered tape, cut to the appropriate size, is held just above the warm corrugation mold, while the top half of the mold is lowered to engage the corrugations. The top half of the mold is lowered until the entire corrugated tape has been formed between the two half molds. The mold is then cooled to room temperature, the top of the mold is removed, and the corrugated tape is stripped from the mold. The corrugations formed in this manner are rigid enough to maintain their shape while the layers are being stacked to form the MSOFC (Fig. 8).

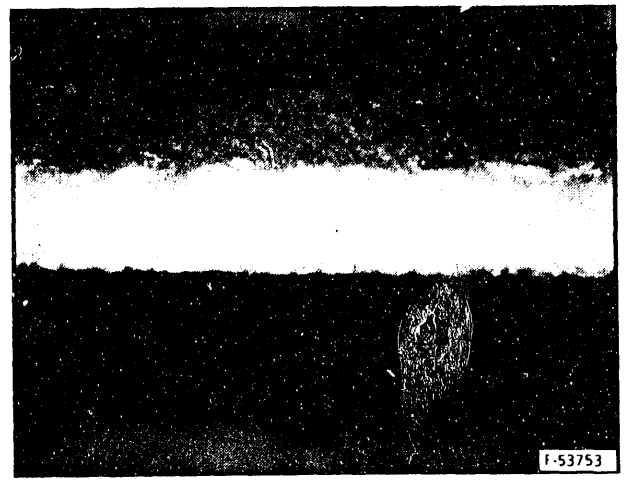

Fig. 6. Photograph of cross section of green trilayer tape fabricated by hot-rolled calendering. (Photo courtesy of Allied-Signal Aerospace Co., AiResearch Los Angeles Division.)

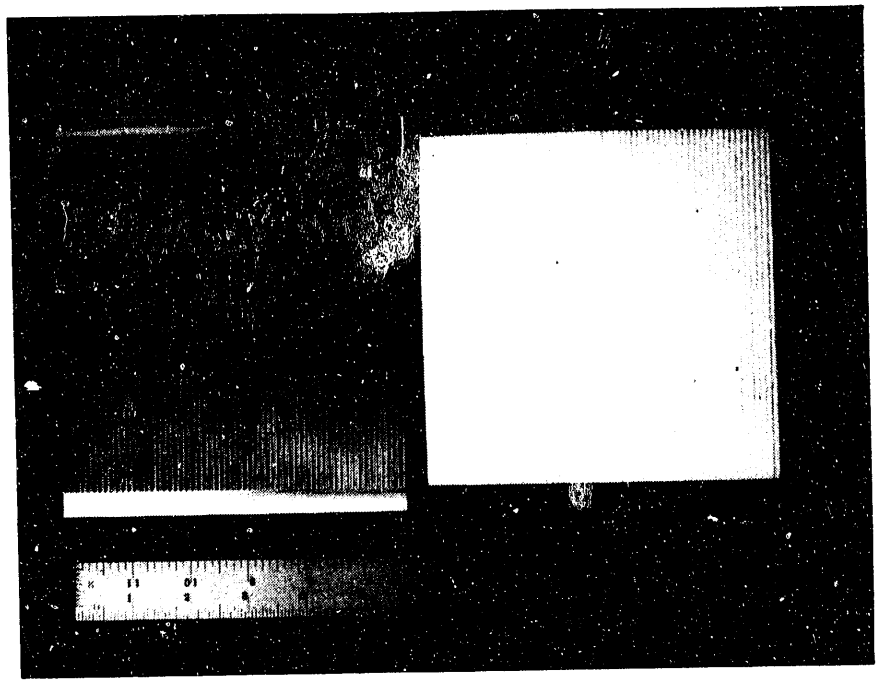

Fig. 7. Photograph of mold used to produce fuel and oxidant channels. (Photo courtesy of Allied-Signal Aerospace Co., AiResearch Los Angeles Division.)

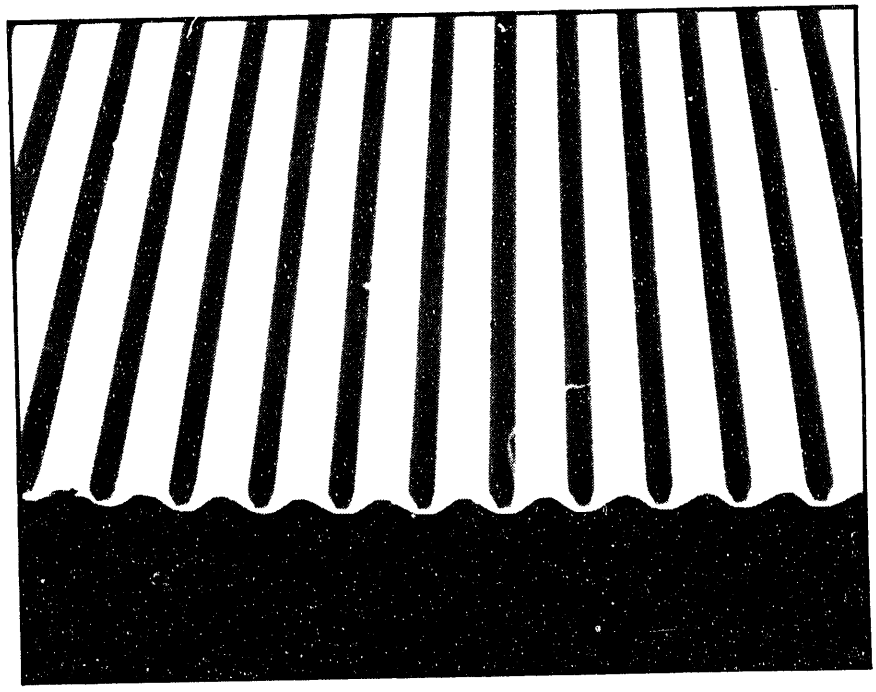

Fig. 8. Photograph of corrugated tape formed by compression molding. (Photo courtesy of Allied-Signal Aerospace Co., AiResearch Los Angeles Division.)

The corrugation method described above has several drawbacks for use in large-size and large-scale production. The method, for example, can stretch the materials over the radius points, resulting in local nonuniformity of component layer thickness as well as introducing residual stresses.

Discussion of Component Properties

The compositions and densities of each MSOFC component are given in Table 2, and tape thicknesses are given in Table 3.

Anode. The anode occurs in the crossflow design as both a planar layer and a corrugated layer. It is a porous (75% theoretical density) structure whose composition is a mixture of nickel oxide and YSZ, which reduces to a cermet of nickel and yttria-zirconia in-situ under the reducing atmosphere of the fuel cell. The 25 vol.% porosity in the sintered tape is of the open variety.

Electrolyte. Electrolyte occurs only in a planar trilayer in the crossflow design. The thickness and the thickness ratio of the trilayer tapes with electrolytes were listed in Table 3. The electrolyte formulation includes an organic binder and a plasticizer. The YSZ, representing 84 wt.% of the green mix and 100 wt.% of the sintered layer, has been identified as a fully stabilized zirconia (8% Y_2O_3 – ZrO_2).

As with the anode, the "organics" are proprietary. The electrolyte is an impervious (95-100% TD) solid ionic conductor with a TD of ≈6.0 g/cm^3. The porosity in the less than fully dense material (5 vol.%) is of the closed type.

The electrolyte layer in the MSOFC crossflow design is made by cocalendering with the anode and cathode tapes before to cutting to size. The electrolyte must be of a high density and crackfree; open porosity or cracks will cause a chemical "short" with loss of efficiency. For the crossflow design, the ratio of electrolyte-to-electrode thickness is 5:1. The electrolyte will be the strongest or load-bearing member of the trilayer.

Table 2. Tape compositions and densities

Component	Tape Formulation	Weight %	Green Density (g/cm^3)	Sintered Density (g/cm^3)
Electrolyte	Yttria–Zirconia	84.0		
	Binder	8.0	3.56	6.00
	Plasticizer	8.0	(59% TD)[a]	(100% TD)
	Solvent			
Cathode	$SrLaMnO_3$	79.6		
	Poreformer	4.0		
	Binder	8.2	3.44	5.20
	Plasticizer	8.2	(50% TD)	(75% TD; TD = 6.84)
	Solvent			
Anode	Yttria–Zirconia	26.6		
	NiO	43.3		
	Additive	5.4		
	Poreformer	6.0	3.02	5.04
	Binder	9.3	(47% TD)	(75% TD; TD = 6.38)
	Plasticizer	9.3		
	Solvent[b]			
Interconnect	$SrLaCrO_3$	85.6		
	Binder	7.2	3.89	6.66
	Plasticizer	7.2	(58% TD)	(100% TD)
	Solvent[b]			

[a]TD = theoretical density.

[b]Added to achieve consistency.

Table 3. Tape thickness for crossflow design

Tape Design and Component	Green Tape Thickness Trilayer Planar in.	Green Tape Thickness Trilayer Planar µm	Thickness Ratio	Total (µm)
Trilayer Planar				
Anode	0.0017	44		
Electrolyte	0.0086	217	1:5:1	305
Cathode	0.0017	44		
Anode	0.0048	122		
Interconnect	0.0024	61	2:1:2	305
Cathode	0.0048	122		
Single-Layer Corrugated				
Anode	0.012	305		305
Cathode	0.012	305		305

Cathode. The cathode occurs in the crossflow design as both a planar layer and a corrugated layer similar to the anode. It is a 75% TD porous electronic conductor with a TD of ≈ 6.84 g/cm^3. The 25 vol.% of porosity will be of the open variety. Sinterability of this oxidant electrode is high at the sintering temperature of interest, and this causes some problems of porosity control.

Interconnect. The interconnect occurs only as a planar trilayer in the crossflow design, similar to the electrolyte. The interconnect formulation also includes organic binder and plasticizers. The strontium-doped lanthanum chromite represents 85.6 wt.% of the green mix and 100 wt.% of the sintered tape in a fully dense, impervious layer.

The interconnect requires high electronic conductivity in both oxidizing and reducing environments. In the sintered state, the interconnect is a fully dense (95-100% TD) impervious electronic conductive perovskite with a TD of approximately 6.66 g/cm^3.

Discussion of Manifolding

Once several individual "cells" have been produced either by cofiring together or by adhesive bonding (see Fig. 9), a method of manifolding is necessary to transport fuel and oxidant. Two basic ideas are selected for manifolding: external and internal.

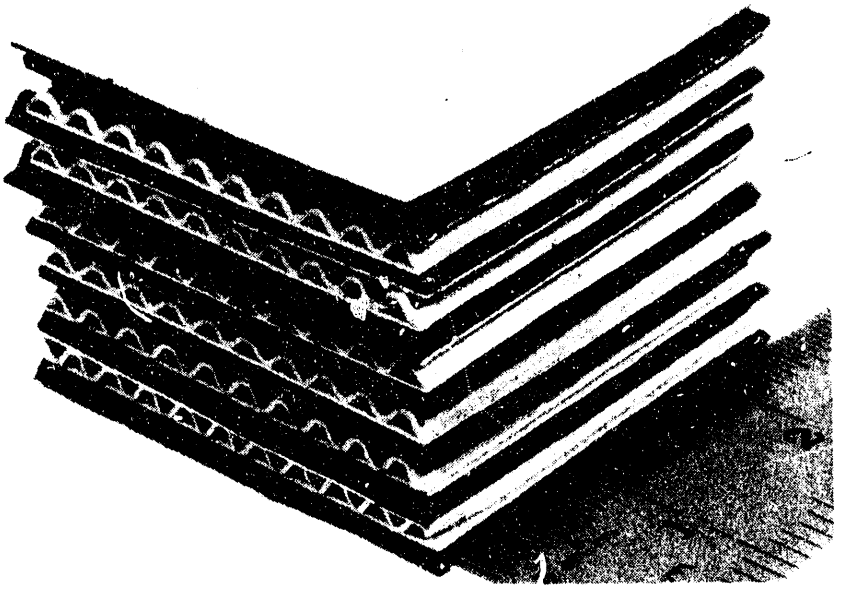

Fig. 9. Photograph of several crossflow "cells" stacked together. (Photo courtesy of Allied-Signal Aerospace Co., AiResearch Los Angeles Division.)

External Manifolding. Figure 10 shows a simplified conceptual design of a crossflow MSOFC with externally manifolding formed by cementing presintered cavity-type panels to the four faces of a "stack." Bus-bar connections of some type would be cemented to the upper and lower faces of the stack for series connections to form a module. Such a stack has the advantages of simplicity and the possibility of modifications to the gas panel design to include an encased multistack build-up.

Internal Manifolding. The second possible manifolding concept is shown in Fig. 11. Present logic suggests that if such an internally manifolded crossflow MSOFC were considered for manufacture, the manifold would be constructed from alternate layers of electrolyte and interconnect with inserts of anode and cathode planar and corrugated layers.

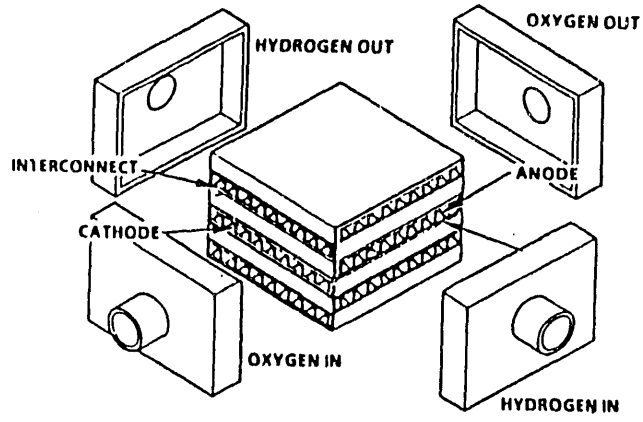

Fig. 10. External manifolding concept for crossflow design

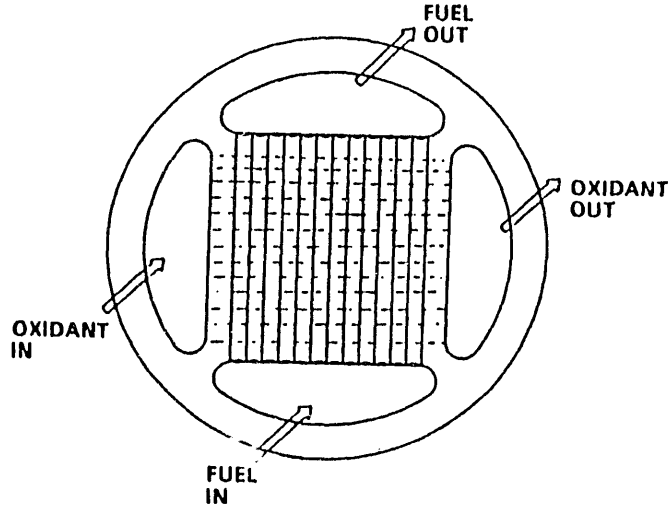

Fig. 11. Schematic diagram of internally manifolded crossflow stack, showing manifold design

3 DETAILS OF CERAMIC PROCESSING, AND SUGGESTED NONDESTRUCTIVE CHARACTERIZATION METHODS FOR EACH PROCESSING STEP

In the previous sections, the basics of fabrication of fuel cell components were outlined. We now consider an approach for nondestructive detection of characteristics and defects of interest. We discuss these in the four major material categories or fabrication steps:

- Powders and Organic Additives.
- Blended Materials.
- As-Calendered Tapes.
- Debindering and Sintering.

For each of the four, a nondestructive characterization (NDC) approach is suggested and briefly described. Where appropriate or possible, example data are given.

Powders and Organic Additives

Powders

The quality and characteristics of starting powders are directly related to the quality and uniformity of the final component(s). Smaller particle sizes (<5-10 μm) result in higher surface areas, but usually require excessive organic binder and plasticizer to coat each small particle for tape production. The resulting high organic content means that the solid loading will be low in the green tape. Consequently, a high density is more difficult to achieve during sintering. On the other hand, larger particles (>5-10 μm) may not have sufficient sinterability under achieveable sintering conditions. Thus, the original powder characteristics of particle size, particle-size distribution, surface area, morphology, etc., affect the fabrication process in many significant ways, including (a) influencing the amount of organic binders and plasticizers required to form the green tape, (b) influencing the porosity of the green tapes, (c) affecting sintering behavior, and (d) influencing final porosity and ceramic-component microstructure. The original powder characteristics must be tailored and optimized for each fuel cell layer. Physical characteristics of a powder are of prime importance, and their effects on part fabrication and quality are listed below.

- Large surface area/small particle size:
  Enhances sinterability
- Equiaxed crystallites:
  Improves packing density

- Narrow particle–size distribution:
  Improves uniformity of microstructure

The larger the surface area, the greater the surface activity, and consequently, the greater the sinterability (which is proportional to the surface activity) of the powder. However, there are practical limits to this.

Small particle size and a narrow particle–size distribution usually results in a homogeneous microstructure. This is desirable because, in general, mechanical strength is inversely related to inhomogeneous microstructures, i.e., for the same material the mechanical strength is greater as the grain size of the ceramic is reduced.

Four groups of starting materials are used in the MSOFC:

- Yttria-stabilized zirconia (YSZ) powder for electrolytes and anodes.
- Strontium-doped lanthanum manganite ($SrLaMnO_3$) powder for cathodes.
- Strontium-doped lanthanum chromite ($SrLaCrO_3$) powder for interconnects.
- Nickel oxide (NiO) powder, also for anodes.

In each case, appropriate chemical and physical properties such as surface area, particle size distribution, particle shape, chemical composition, purity, and phase composition are necessary. Comments on nondestructive characterization needs relative to each powder for each component are discussed in the context of a review of each component.

Anode Powder. The formulation for the anode was given in Table 2. The anode powder, YSZ-NiO, is readily available and does not present a large source–variability problem. No special NDC effort is currently recommended.

Cathode Powder. The formulation for the cathode was given in Table 2. Although different formulations are used, one such formulation is $Sr_{0.1}La_{0.9}MnO_3$. The cathode is a 75% TD porous electronic conductor with

a TD of 6.8 g/cm^3. Sources of $SrLaMnO_3$ powder for the cathode are not readily available, and great care should be taken in the NDC of this powder.

Interconnect Powder. The formulation for the interconnect was given in Table 2. Although many formulations are given, one interconnect formulation could be $Sr_{0.1}La_{0.9}CrO_3$. Sources of $SrLaMnO_3$ powder for the cathode are not readily available, and we believe that great care should be taken in characterizing this powder.

Electrolyte Powder. The formulation for the electrolyte was given in Table 2. The YSZ has been identified as fully stabilized zirconia (8% Y_2O_3-ZrO_2).

Suggested NDC Methods for Powders

Of the four powders, YSZ and NiO are commercially available and of high quality, while $SrLaMnO_3$ and $SrLaCrO_3$ are not and thus deserve the most attention. Powders are extremely important, and the parameters listed below must be measured.

Crystallographic Phases

By far, the predominant NDC technique for crystallographic phase measurement is X-ray diffraction because of its ease, convenience, speed, and the wealth of information it provides.[11] *Other methods include infrafred (IR) and Raman spectroscopy.*[12] *Nuclear magnetic resonance (NMR) cannot be used because none of the nuclei are NMR-sensitive.*[13] *The other methods are used primarily to determine phase ratios, with IR spectroscopy currently the most prevalent. Raman spectroscopy is used rarely because of limited instrument availability but is demonstrably useful in that very small fractions of a phase may be identified.*

An advantage of the X-ray diffraction pattern is that it immediately identifies the presence of the desired material; that is, it answers the question of whether the powder is really what it is supposed to be. It also provides quantitative information on the relative amounts of the phases and on the extent of powder crystallinity. The presence of major impurities can also be immediately deduced from X-ray diffraction data.

Chemical analysis of a powder is often used to establish the feasibility, reproducibility, and consistency of a synthesis technique to produce powders. The two most prevalent techniques for the determination of metallic impurities are emission spectrometry (ES) and atomic absorption (AA).[14]

Foreign Particles

The tolerance levels for metallic impurities vary, and it is imperative that acceptable contaminants, rather than metallic discrete particles or chunks, be homogeneously dispersed. The deleterious effects of iron have been well established. We suggest that high-magnification X-ray imaging methods using microfocus X-ray sources be used to screen powders for foreign material before characterization or use.

Surface Analysis

Surface analytical methods determine the surface composition and distribution of elemental species. Table 4 lists three instrumental techniques used in surface studies.

Table 4. Surface analytical techniques

Method	Minimum Powder Sample Size (mg)	Detection Limit (%)	Precision (%)	Sampling Depth (Å)
Electron Spectroscopy for Chemical Analysis (ESCA)	25	0.5-1	10-20	20-50
Auger Electron Spectroscopy (AES)	5	0.2	2	20-50
Secondary Ion Mass Spectroscopy (SIMS)	10	0.001	10	5-10

Particle Size and Distribution

Particle–size and particle–size distribution methods are shown below. For fine powders, light scattering is the preferred method. Sedimentation is too slow for fine submicrometer particles, and the measurement may take hours. Examination of electron microscopic images is tedious because it requires several samplings.

- *Method:*
  -Light scattering.
  -Sedimentation.
  -Electron microscopy.
  -Air permeability (assumes monosized spherical particles).

One additional technique provides an estimate of average particle size, but not size distribution:

- *Specific surface area determination by BET, which assumes particle sphericity but has the unique advantage of being independent of agglomeration.*

In evaluating important powder properties, it will be important to use complementary techniques to obtain valid estimates. At the same time, it is not always necessary to determine all of a material's characteristics, only those that pertain to and affect its application. Currently, correlations between powder characteristics and ceramic component performance is not well defined and is an area of intense investigation.

Organic Additives

Organics used as binders, plasticizers, and solvents make up 30 wt.% of all compositions of the cathode, electrolyte, and interconnect and nearly 20 wt.% of the anode. These additives significantly affect processing. It is important to note that from the standpoint of NDC, detailed knowledge of each organic "additive" component is necessary, because each composition gives rise to entirely different NMR spectra that might ultimately be used as a diagnostic.

Suggested NDC Methods for Organic Additives

Although the chemical composition of the organic additives is carefully specified, small quantities of impurities could change the behavior of the important powder-additive surface chemistry routine. NMR and FTIR spectroscopic methods can be used to validate the uniformity of the chemical compositions of the organic additives.

Blended Materials

Blending

Previous research has shown that it is critical to introduce the dispersing agent independent of other polymers in order to prevent competition for the ceramic particulate surfaces and therefore to produce more uniform viscosities in the slurry.

Additional work has shown that adding the plasticizers to the mill prior to the binder addition aids in the dissolution of the binder into the overall slurry. It is believed that this is due to the preferred solubility of the binder in the plasticizer relative to its solubility in the solvent system. Milling is usually performed in standard ball or jar mills and vibrating mills.

Conditioning

After blending, the slurry is ready to be conditioned for hot-rolled calendering. The conditioning procedure consists of deairing the slurry either by vacuum or by a slow-rolling or agitation step. From an NDC standpoint, some form of characterization of the blended material, likely NMR or FTIR spectroscopy, would be important to establish the completeness of the blending, especially with materials used in the process which have been "recycled" back into the process stream, as well as the differences in local chemistry (i.e., at the powder/matrix interfaces).

Suggested NDC Methods for Blended Materials

The blended materials contain powder, binder, plasticizer, solvents, and additives. Currently, a jar mill is used for initial blending, followed by use of a Banbury mixer for follow-on blending.

Especially critical is the distribution of organics and whether or not the powder surfaces are uniformly covered. We therefore suggest that a comprehensive nondestructive characterization be conducted at this stage (note that there is the possibility of using reclaimed material in full-scale processes).

We suggest that ^{1}H NMR spectroscopy be studied on the blended material to establish details of powder surface chemistry of blended material.

It is significant that rheological properties cannot be correlated to tape stability, density, or sinterability. Further, as noted in later sections of this report, blending of recycled materials will become critical in tape uniformity.

As-Calendered Tapes

Because of the need to control the speed and temperature of each counterrotating roller, the potential exists for high shearing across the tape. This creates the potential for significant problems in the tapes. We will discuss here briefly three tape types: single-layer tapes, manifold tapes, and trilayer tapes.

Single-Layer Anode and Cathode Tapes

Anode and cathode tapes are made in two different thicknesses. Case 1 is a single 305-μm-thick layer that is subsequently "corrugated" to form fuel channels, and Case 2 is as part of the 305-μm total thickness trilayer flat material.

After calendering, the tapes are placed on curing trays (a low-heat facility) for a time. This allows evaporatation of a high fraction of the additives and solvents from the tape.

For crossflow designs, the tape intended for corrugation is then cut (stamped) from the larger green tape. Because of the rolling operation, there can be a tendency to have a "built-in" memory in the polymeric additives, which will "remember" the rolling direction. It is likely that a preferred orientation would affect stresses and the sintering reliability of

the tape. Thus, it will be necessary to check the anisotropy of the residual stresses in the tape at this point.

Formation of Fuel and Oxidant Channels. While still in the green state, the tape is formed with corrugations. Figure 12 shows the dimensions of the corrugations as currently used. The corrugations are formed in a two-part mold. Because of stretching of the tape over the radii, some concern can be expressed about development of residual stresses at the curvature points. If the thickness of the fuel channels affects overall stress levels in a stack, or if crushing strength is greatly affected, then thickness must be carefully monitored.

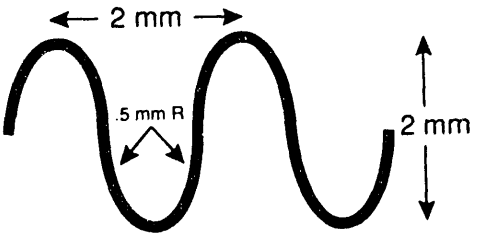

Fig. 12. Schematic diagram of anode corrugation pattern

Suggested NDC Methods for Single-Layer Tapes

We believe that the highest-priority NDC activity is necessary at the as-calendered step. For single 305-μm-thick tape, what is needed is assessment of (a) thickness uniformity to ±5% or ±30 μm; (b) density uniformity to as-yet-unspecified values (recent data suggest that a ±3% variation will yield a ±20-30% change in biaxial strength); and (c) distribution of organics, poreformer, and powder, also to as-yet-unspecified values (related work on injection molding suggests that ±10 wt.% is significant).

Thickness Uniformity

We suggest that the NDC method known as pulse-echo c-scan ultrasonics, with use of a transducer array, be studied as a thickness-measuring system.[15,16] *The system will allow the first-surface and backsurface reflections to be obtained. This will yield total thickness (with proper calibration), as well as some material characterization such as organic/powder ratio or density, with*

proper signal processing and calibration. Several items should be mentioned in this recommendation. First is the sensitivity to thickness. Recall that for sound velocities in solids,

$$\frac{c}{f} = \lambda$$

where:

c = the sound speed in the solid (mm/s),

f = frequency (Hz), and

λ = wavelength (mm).

For green ceramics, very little data are available in the literature on either longitudinal or shear wave velocities. Further, because of the visco-elastic properties of green ceramics, one must consider non-linear wave propagations. We will consider here only longitudinal velocities because significant problems[17] are encountered when attempting to couple shear wave transducers onto green ceramics.

If we assume that the green ceramic longitudinal sound speed will be between 800 and 1600 m/s, and if we want a wavelength of 30 μm, this will dictate a frequency of 25 to 50 MHz.

Recall, however, that both anode and cathode require a significant amount of poreformer to achieve 20 to 50% porosity and thus ensure that sufficient oxygen reaches the electroactive region at the air electrode/electrolyte interface. The lower limit of porosity is set by current conditions. The upper limit of porosity is determined from considerations of array strength. This amount of poreformer may cause significant ultrasonic attenuation.[18-20] However, because the total tape thickness is only 305 μm, the total ultrasonic path length will be 610 μm, so significant attenuation likely can be accommodated. Reported values[18] are on the order of 1-2 dB/mm, thus, for this case, total attention would be only 0.5-1 dB.

Transducer diameter will likely be 4-10 mm. Thus, packing these into a side-by-side array does not present a problem, and electronic methods are available to sequentially interrogate each transducer.

Density Variation

We suggest two methods be studied for measuring density variation: (a) ultrasonics and (b) real-time microfocus X-ray radiation (with either an image intensifier/CCD array or solid-state detector).[21,22]

Ultrasonic methods as described above for thickness measurements can also be used for density measurement. The velocity of a longitudinal ultrasonic wave traveling in a solid can be related to the elastic properties and the density by the relationship

$$V = \left[\frac{E(1 \pm \nu)}{\rho(1+\nu)(1 \pm 2\nu)}\right]^{1/2}$$

where:

V = *sound velocity in the solid (m/s),*

E = *elastic modulus (MPa),*

ν = *Poisson's ratio, and*

ρ = *density (kg/m*^{3}*).*

This holds for truly elastic bodies. However, the green ceramic tape, which is held together by polymeric material, is an elastic-plastic body and therefore the elastic modulus must be determined. Regardless of this, past work has shown that ultrasonic longitudinal velocities can be related to ceramics density to $\pm$*1-2%. Prior work*[17] *has shown that ultrasonic longitudinal velocity can be related to green ceramic density for an MgO specimen containing 20 wt.% polyethylene glycol binder (see Fig. 13). Other work*[23] *has also shown that ultrasonic longitudinal velocity can be related to density variations in partially sintered SiC and that variations in density within a specimen can be detected and verified (see Fig. 14). Thus, use of an ultrasonic c-scan system seems to be possible for measurement of thickness and density.*

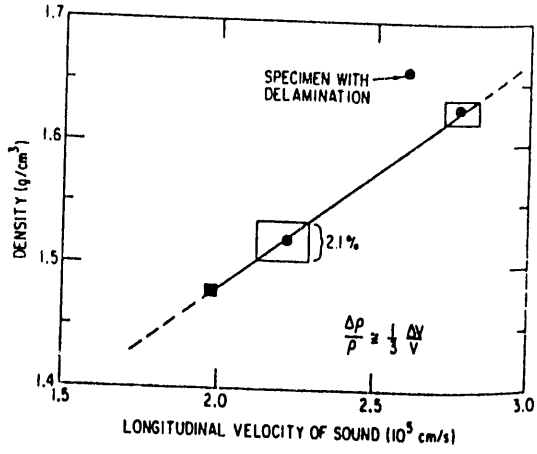

Fig. 13. Ultrasonic, through-transmission velocity measurements as a function of green ceramic density (MgO + polyethylene glycol binder of 20 wt.%) (Ref. 17)

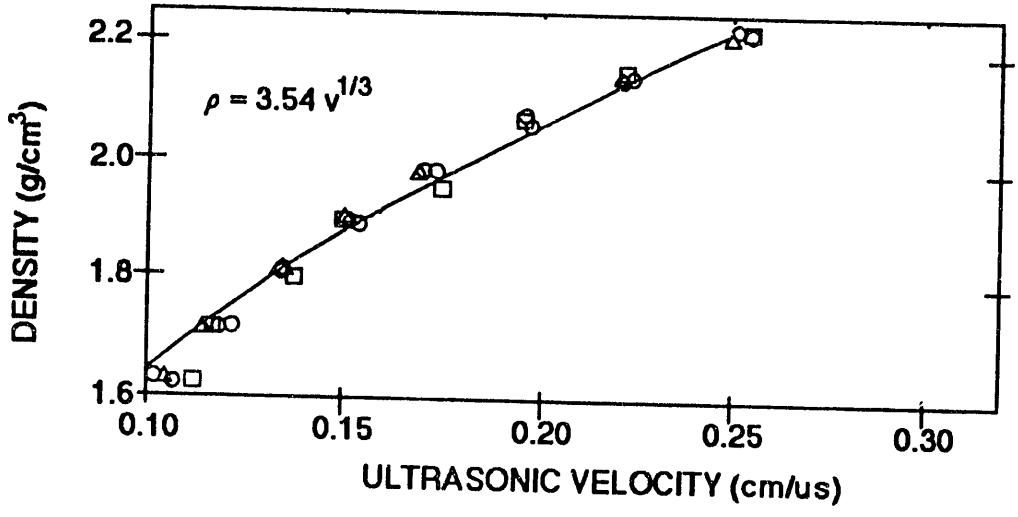

Fig. 14. Ultrasonic, through-transmission velocity measurements as a function of presintered SiC material density (Ref. 23)

The ultrasonic inspection method itself consists of many variants. Major variables relate to the selection of the transducer size, operating frequency, focal length, configuration (one or an array of transducers), inspection on one side or on opposite sides, orientation (normal or angled relative to the surface), and coupling method (immersion, water jet, or contact). The transducer configuration recommended for single-layer tapes consists of normal incidence pulse-echo c-scan. Of all the configurations, this should provide the least sensitivity to surface roughness while maintaining adequate

sensitivity. For the selected approach to be easily scaled for inspection of large parts at high scan speeds, the ultrasonic pulse should be coupled by an acceptable method. Suggested coupling is through a contact method where the transducer array will be in an oil bath contained in a thin membrane that will contact the tape. Small f-number (slightly focused) transducers will be recommended to ensure uniform sensitivity. To create an image of the tape, a grey scale 8-bit (256) or greater with false color representation can be created in real time by writing pixels to a video monitor. Each pixel will represent the maximum or "peak" echo signal amplitude at the corresponding location on the sample.

As for ultrasonic systems, several factors must be considered when using X-ray imaging systems for densitometry.[21] *The basic law of X-ray absorption is given as*

$$I/I_o = exp(-\mu x)$$

where:

I = *detected intensity (photons/cm*^{2}*-s),*

I_o = *source flux (photons/cm*^{2}*-s),*

μ = *linear X-ray attenuation coefficien (cm*$^{-1}$*), and*

x = *dimension of object penetrated by X-ray beam (cm).*

The source flux is dependent upon the source type (X-ray tube, synchrotron, etc.) and the linear attenuation coefficient is dependent upon the material under study and the energy of the X-ray radiation. Conversion of detected intensity to data is dependent upon the specific detector that is used; this is discussed later.

The mass attenuation coefficient, μ_m, *is written as*

$$\mu_m = \mu_{\ell\rho}$$

where:

μ_ℓ = *linear attenuation coefficient* (cm^{-1}), *and*

ρ = *mass density* (g/cm^3).

One can therefore relate I/I_o *to density as*

$$\rho = \left| \frac{\ell n\, I / I_o}{\mu m\, x} \right|$$

Thus, if one can measure the relative intensities and knows the attenuation coefficients, the density can be determined. For a compound, the rule of mixtures can be implemented to obtain μ_m *as*

$$\mu / \rho = \sum_i \rho_i (\mu / \rho)_i$$

where:

ρ_i = *fraction of total weight of the* i^{th} *element.*

Recall, however, that μ_l *is dependent upon the X-ray energy (keV) and that X-ray tubes are polychromatic. Thus, one also must know the flux of the X-ray source to predict density. Depending upon the noise level of the detector, however, densitometry values >1-2% should be achieveable.*

The ability to resolve details in structure using X-ray energies is often studied by the relation

$$\mu x = 2$$

where:

μ = *linear X-ray attenuation coefficient (energy dependent;* cm^{-1}), *and*

x = *depth of penetration.*

Thus, if one knows the linear attenuation coefficient of a material and the thickness, the optimum X-ray energy can be established. Recent work[26,27] has been conducted to establish optimum X-ray energy for each of the fuel cell components, i.e., anode, cathode, electrolyte, and interconnect, for both as-cast (green-state) and densified conditions (see Fig. 15).

Porosity

We suggest that porosity distribution (or rather, poreformer distribution at this stage) be detected by ultrasonic pulse-echo c-scan methods with focused transducers. Recall that ultrasonic longitudinal velocity, V, was related to elastic modulus. However, past work[24] has suggested that the elastic modulus can be related to pore fraction. This work was done on sintered ceramics, however, and we suggest that analysis of the ultrasonic signals be conducted as part of a two-phase material analysis. An example of how ultrasonic longitudinal velocity can be related to porosity in partially densified Si_3N_4 is shown in Fig. 16.

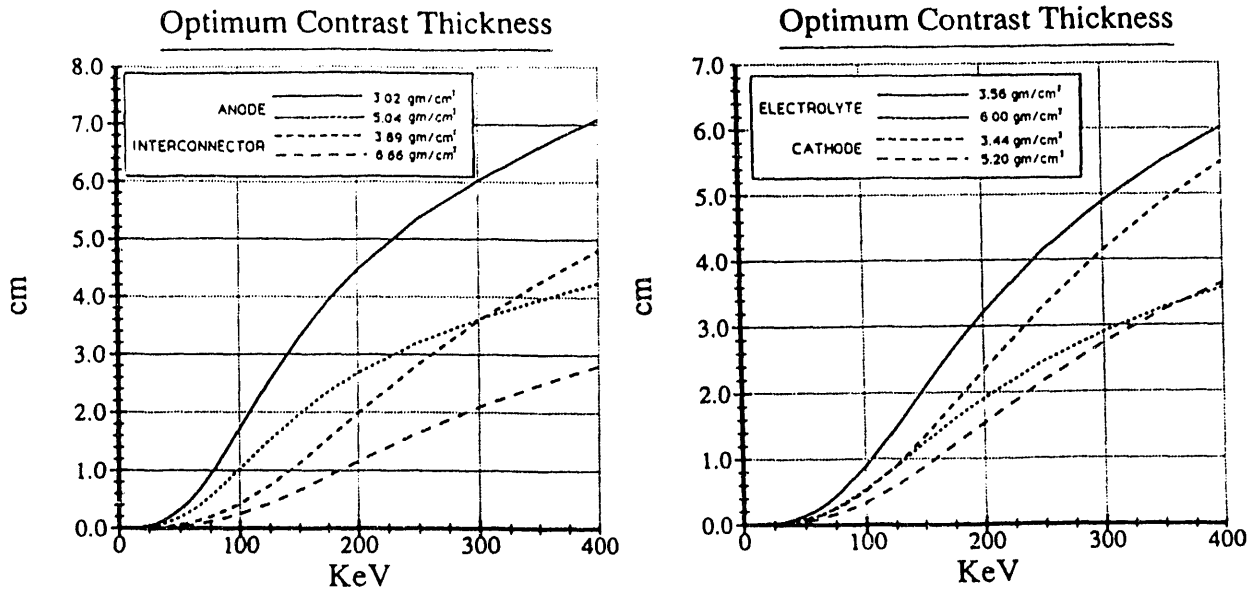

Fig. 15. Optimum X-ray energy for maximum image contrast for as-cast (green-state) and dense individual fuel cell components

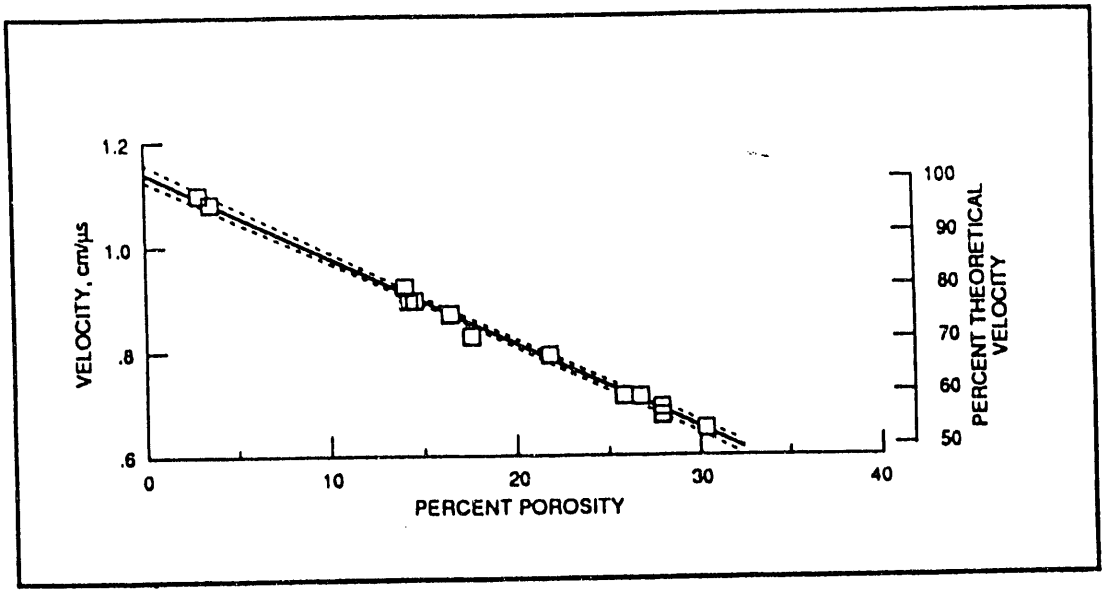

Fig. 16. *Longitudinal velocity vs. percent porosity for Si_3N_4. Velocity = -0.016 x percent porosity + 1.14. Percent theoretical velocity = -1.41 x percent porosity + 100. Correlation coefficient = -0.997.*

Large Pores, Inclusions

We suggest that real-time X-ray microfocus radiography be employed.

Residual Stresses in Corrugated Types

Because of the likelihood of potentially large residual stresses developing during corrugation, we suggest an effort to measure these in the green state. Until very recently, the ability to measure residual stresses in polymeric materials was limited and no systematic work had been reported. Recently, however, Mendoza and Cannon[25] reported that Fourier transform infrared (FTIR) methods can be used to map residual stresses in injection-molded green ceramics that use polymeric material as the binder.

Manifold Tapes

The manifold for the crossflow design currently consists essentially of four box-type manifolds that can be cemented onto the stack after sintering.

These manifolds will be made by press forming pug-mill-extruded tape into a four-sided box with a gas–conduit aperture. At this time, the material of choice for the manifold is YSZ, with the majority of this material originating in the electrolyte process.

Because the primary purpose of the manifold is gas containment, it must be a fully dense, gas–impermeable structure. Therefore, NDC requirements must focus primarily on large entrapped air bubbles that could cause gas leakage. It has been suggested that acceptable leakage rates are 0.1 vol.% after manifolding for H_2 fuels, and <5 vol.% for the oxidant.

Suggested NDC Methods for Manifold Tapes

We suggest that manifold tapes be examined by pulse-echo c-scan ultrasonic methods, as well as by real-time microfocus X-ray, just as would be done for the single–layer anode and cathode tapes.

Trilayer A/E/C and A/I/C Tapes

For trilayer tape manufacturing, the anode and cathode must be co-rolled with either an A/E/C combination or an A/I/C combination. In the former, the trilayer thickness ratios are 1:5:1 and total thickness is 305 μm. Each layer has a thickness, in order, of 44 μm, 217 μm, and 44 μmm. In the latter case (A/I/C), the thickness ratio is 2:1:2; thus, the thickness of each layer, in order, is 122 μm, 61 μm, and 122 μm. Again, total thickness is 305 μm.

Single–layer anodes and cathodes are calendered with sufficient size to satisfy a single crossflow stack design and are corolled with an equivalent electrolyte tape in one case and interconnector tape in the other case. The continuous trilayer tapes are cut to size for the designed power stack, accounting for the ≈20 linear percent shrinkage. All waste trimmings are currently planned to be returned for recycling at this point. Note that this will place a great demand on the NDC process at the blending operation to ensure reliable and uniform material before extrusion.

Interconnect. The interconnect is always sandwiched between an anode and a cathode. Because the interconnect must be crack-free and impervious to gases, no trapped air bubbles or nonuniformities (which could

act as flow regions during sintering) should be present in the as-calendered tape.

A significant point about the interconnect is that it is processed from $SrLaCrO_3$ powder. It was noted earlier that supplies of this powder are limited and that therefore reliability is a problem. Hence, as-calendered tapes for the interconnect deserve significant NDE attention.

At a thickness ratio of 2:1:2 for an A/I/C-E trilayer and a total green state thickness of 305 μm, the interconnect is only 61 μm thick in the green state. This is extremely important because many applicable NDC methods, e.g., acoustic microscopy, will have significant sensitivity to thickness. From an NDC standpoint, the density distribution, thickness distribution, and organic distribution must all be brought to critical measurement sensitivity on the interconnect.

Electrolyte. As with the interconnect, the electrolyte in a crossflow MSOFC design is always sandwiched between an anode and a cathode. Unlike the interconnect, however, the electrolyte is made of a readily available powder, i.e., PSZ. Hence, problems with significant nonuniformities are likely to be fewer. The electrolyte, like the interconnect must be impervious to gases in the dense state, and thus there is a great need for sensitivity in the as-calendered tape to density variations, organic nonuniformity, and thickness sensitivity (which might cause nonuniform shrinkage).

Suggested NDC Methods for Trilayer Tapes

We suggest that an additional NDC method be developed for the trilayer tapes. That method is time-resolved-infrared-radiometry (TRIR).[26-30] *We suggest that this passive sensing system be implemented immediately downstream of the hot-roll calender. Both sides of the trilayer should be imaged with the TRIR method. This will likely provide information on gross defects (>1-2 mm), including internal tape voids.*

The basic idea behind passive TRIR imaging is that the surface temperature is influenced by homogeneity of the material, thermal diffusitivity, and time. Changes in surface temperature can be considered as a contrast in the resulting image, which is a transient.

Determination of time dependence of the change has been suggested[26] as

$$t_{1/2} = 1.38L^2/\pi^2 k$$

where:

$t_{1/2}$ = time for surface temperature to reach 1/2 peak or minimum value (sec),

L = specimen thickness (μm), and

k = thermal diffusivity, which is unknown for green ceramics, has values of 0.4-1 x 10^{-6} m^2s^{-1} for graphite–reinforced plastics.

For glass–reinforced plastics, $t_{1/2}$ has a value of about 100 sec. Because the anode would be on one side and the cathode on the other, each would have a different diffusivity constant. Correlations likely could be drawn by proper image processing.

The detectable defect size is suggested to be an area with a diameter approximately equal to twice the thickness of the layer being interrogated. For A/I/C, this would be ≈220 μm, and for A/E/C, ≈90 μm.

We also suggest that a pulse-echo c-scan ultrasonic system be developed that, as opposed to the single-layer tapes, will use transducer arrays on both sides of the trilayer tape. This will provide thickness and perhaps density data on both A and C, and by subtraction or direct reflection, thickness of the internal layer. Recall, however, that for a wavelength equal to 0.1, the thickness for the green tapes (≈30 μm), a frequency of 25-50 MHz would be required. For the 2:1:2, A/I/C/trilayer, this would also be acceptable. However, for the 1:5:1 A/E/C, with 44 μm electrode thicknesses, a much higher frequency (≈100 MHz) may be necessary.

We also suggest that through-transmission microfocus X-ray imaging be employed because of its ability to directly detect voids, cracks, etc.

Debindering and Sintering

There are several alternatives to the steps to densify the complete stack. These include (a) densifying individual cells (i.e., anode fuel channels, an A/E/C layer and cathode channels) and interconnect separately and then bonding them together or (b) making a complete stack and sintering all at the same time (this is called cosintering). In the first case, if the interconnect can be sintered separately, then subassemblies of fuel-channel anodes, electrolytes, and oxidant channel cathodes could be inspected separately and the important interconnect could be thoroughly inspected as a single flat piece. In the second case, for a 25 kWe stack, there are 109 A/I/C layers and 109 A/E/C layers, which are all sandwiched with no direct access. This will essentially preclude NDC detection of individual microcracks or delaminations of the electrolyte or interconnector. In either approach, there are two steps: (a) debindering (i.e., removing the organics) and (b) final sintering (final densification).

Debindering

Debindering is the process of heating the green ceramic from room temperature to 500-600°C, during which all the organics (solvents, binders, and additives) are removed. The mechanisms of the debindering process are still not fully understood, according to processing developers.

It must be noted, however, that removal of the organics from a complete stack of cells for a 25 kWe stack weighing 80 kg (including ≈30 kg of organics) will be a formidable task when superimposed upon the purely thermal degradation of the binders. Furnace temperature profiles and the heat transfer of the stack must be controlled so that no points in the stack differ in temperature by more than ±5°C; this prevents relative shrinking between tape and layers of more than ±3%. Deviations from these acceptable "temperature windows" could cause cracking or delaminations between layers or severe dimensional instabilities.

Two basic types of cracking are (a) total delamination between tape types (see Fig. 17) and (b) in-plane cracking of one of the trilayers, usually the electrolyte or the interconnect (see Fig. 18).

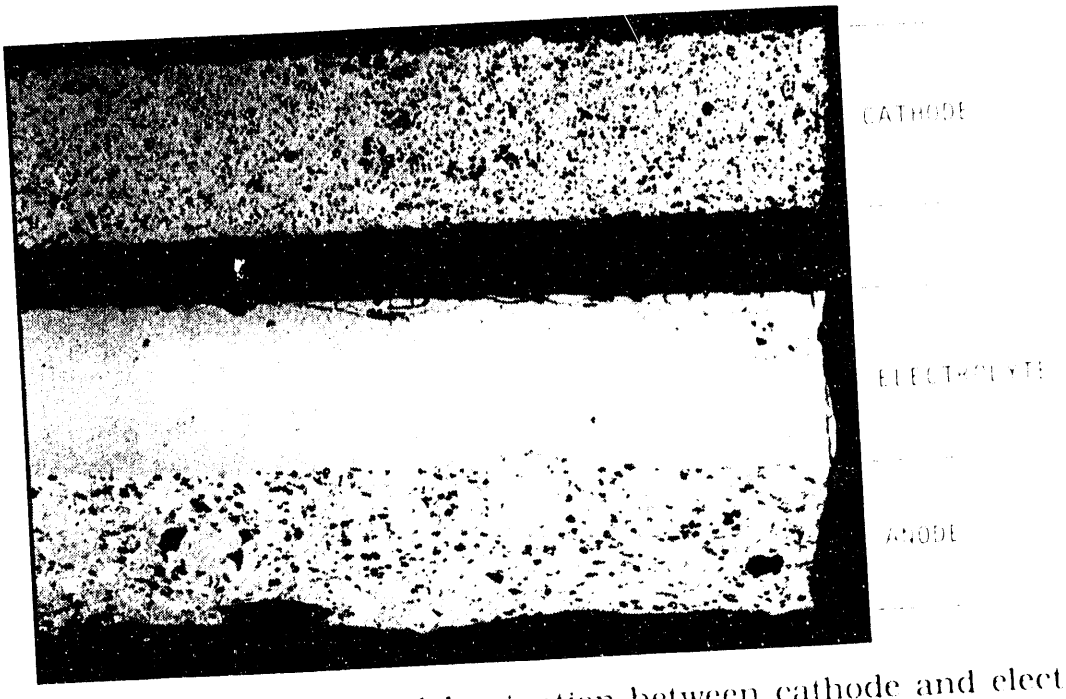

Fig. 17. Photograph showing delamination between cathode and electrolyte layers. (Photo courtesy of Allied–Signal Aerospace Co., AiResearch Los Angeles Division.)

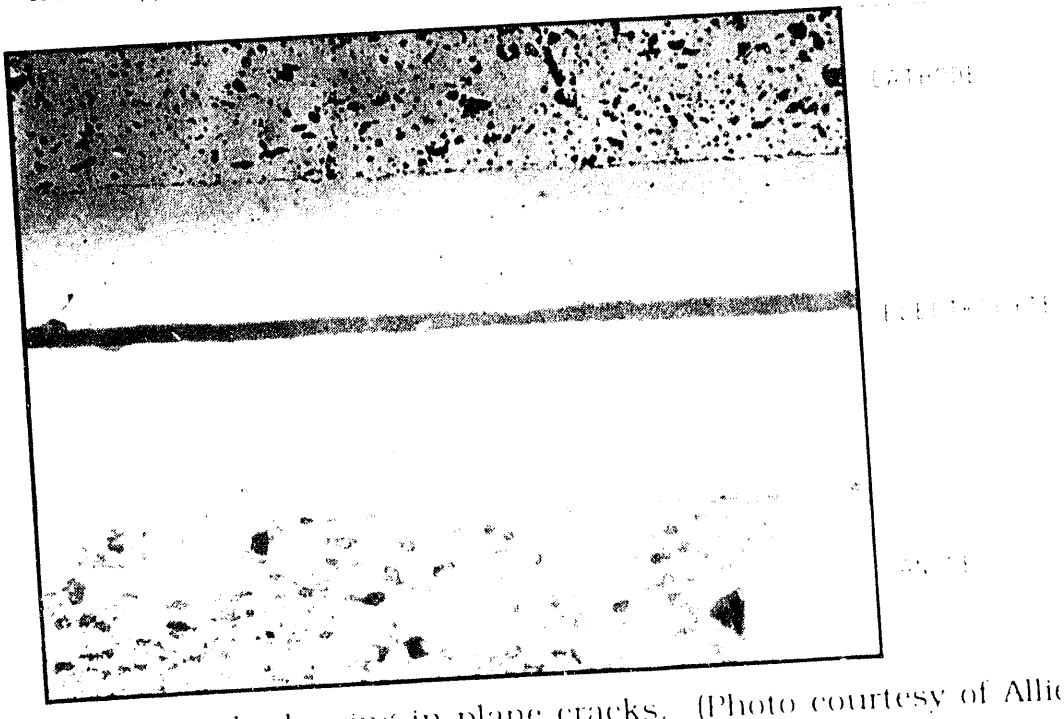

Fig. 18. Photograph showing in-plane cracks. (Photo courtesy of Allied Signal Aerospace Co., AiResearch Los Angeles Division.)

The temperature ramp from room temperature to 600 C will need to be developed, and the temperature regimes for maximum organic removal from individual or combined tapes also must be determined.

Recent work with dilatometers has revealed significant shrinkage during debindering. The small contribution of 3-5 linear percent within the overall total shrinkage of 20-25% may be enough to create internal stresses[31] that lead to delaminations or cracking.

A debindering period of 24-30 hr has been suggested for a full stack during cosintering. This can change if the individual components are sintered and then bonded.

Final Sintering

In the cosintering case, the sintering step is critical because the stack can be very fragile at this point in the process. The stack would need to remain on an appropriate support for transport to the sintering furnace. The fragile nature of such stacks can be seen in Fig. 19, which shows how corrugations can collapse after debindering and during cosintering. These problems can probably be eliminated if the individual components are sintered separately and then bonded together.

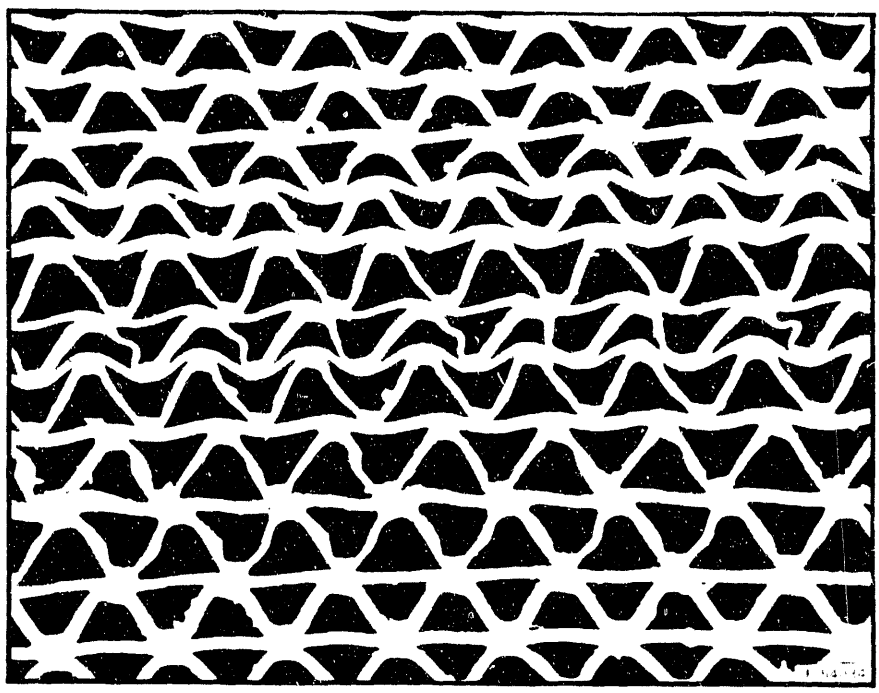

Fig. 19. Photograph of cross section of a stack showing how corrugations can collapse during processing. (Photo courtesy of Allied-Signal Aerospace Co., AiResearch Los Angeles Division.)

The thermal ramp up to the sintering temperature for either a complete stack (in the case of cosintering) or for each component will be quite different than that for debindering because of the absence of outgassing organic materials. However, as with the debindering step, temperature uniformity must be maintained to minimize temperature gradients. Each of the individual components (anode, cathode, electrolyte, and interconnect) has its own sintering profile.

Heat-up is one part of the ramp. Cool-down is equally, if not more, important. On cool-down from the sintering temperature, any thermal expansion mismatch in a component can cause significant internal microcracking. *The sintering stage in the MSOFC manufacturing process currently is the most critical and highest-risk stage in the entire fabrication process. One failed cell, which could be caused by a single failed component, within a stack causes the whole stack to fail.* It is for this reason that an acoustic-emission NDC development program is recommended for detection of the onset of such undesireable cracking. This approach is discussed below.

Suggested NDC Methods for Debindering and Sintering

After a sintered fuel cell stack is removed from the furnace, cracks may be detected, but it is not known when these cracks develop (i.e., during heat-up or cool-down). Knowledge of when the cracks occur could be used to modify heat-up and cool-down schedules so as to minimize cracking. Acoustic emission (AE) is a passive monitoring method that is well suited to the detection of incipient cracking in inaccessible locations such as the inside of the furnace. In previous work, efforts were devoted toward implementing AE methods to detect onset of cracking during sintering of fuel cell arrays.*

Figure 20 is a block diagram of an AE instrumentation system that can be employed. The primary problem in a high-temperature AE test setup is acceptable acoustic coupling of the monitored object to the AE transducer.

---

*Acoustic emission is defined as a transient elastic wave generated by the rapid release and/or transmission of energy from a localized source or leak within a material.

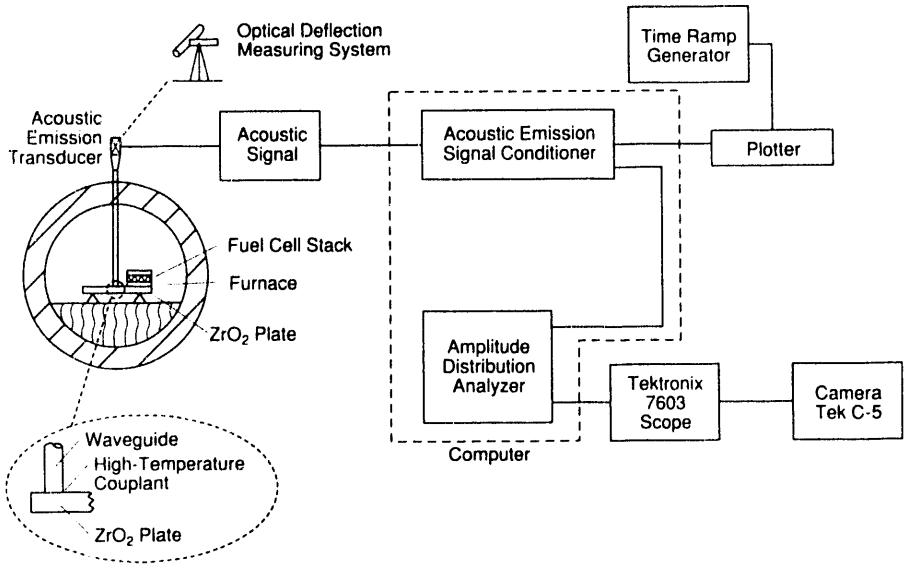

Fig. 20. Schematic diagram of acoustic emission sensing system for detection of cracks and/or delamination in fuel cells during debindering and sintering

Two different coupling methods have been previously tested. In the first method, a 3.5-mm-diameter quartz waveguide was coupled to a zirconia base plate (used to support the fuel cell during debindering and sintering) by contact pressure with a high-temperature couplant. These results suggested that the amplitude of the AE signals was too low (i.e., attenuation was too high at the contact), and thus a new coupling system (see Fig. 21) was implemented.

In this system, a quartz waveguide is fused to a 2.5-mm-thick quartz plate that in turn rests directly on top of the fuel cell component. The fuel cell was placed on a 2.5-mm-thick quartz plate supported on three-point-contact supports. Care was taken to ensure that the upper quartz plate was normal to the waveguide and that this plate was parallel to the lower quartz plate so that no distortion or nonuniform load on the fuel cell could be attributable to plate misalignment.

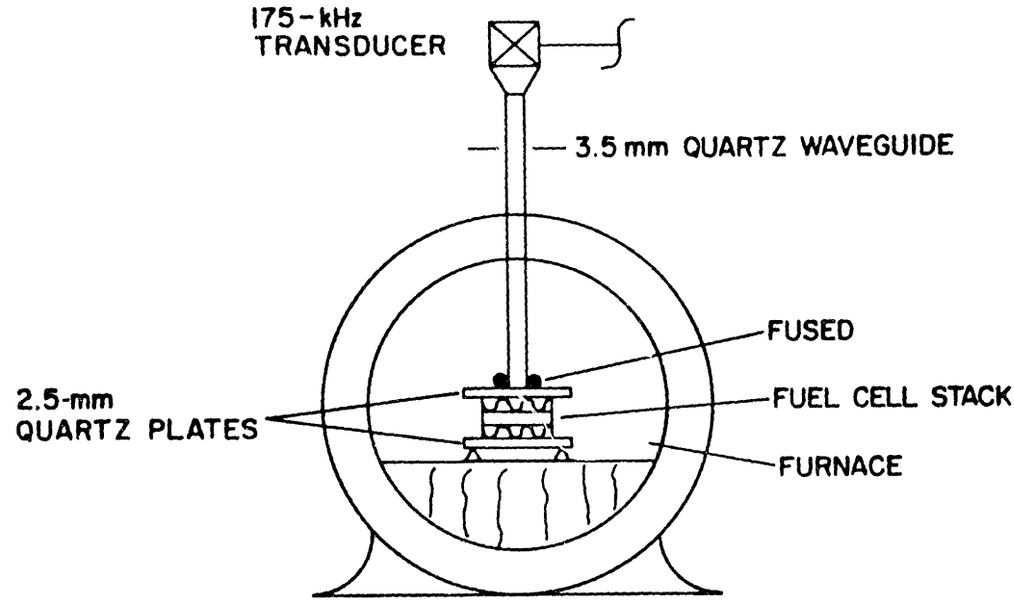

Fig. 21. Schematic diagram of a second high-temperature acoustic emission coupling arrangement

The temperature ramp used for the AE test was an accelerated heat-up ramp with a normal cooling rate. Figure 22 shows the heat-up and cool-down curves, together with the detected AE activity. Note that the AE activity occurred at only three temperature regions, i.e., approximately 400-500°C, 600°C, and from 1350°C to the end of the 1400°C hold cycle. The relative strength of the detected emissions can be assessed by amplitude distribution analysis. Time-dependent amplitude distributions were obtained on this test run, and the data (Fig. 23) show the changes in distributions from the previous measurement. To be noted is that the level of AE activity at 1300-1400°C is dramatically revealed by the amplitude distribution plots. The relative strength of the pulses increases near 1400°C.

After the run, inspection verified that the sample had totally collapsed, as suggested by the deflection data and the significant AE activity at 1400°C. It was concluded that the AE was detecting the collapse of the cell. This suggests that this method, when the experimental setup is properly arranged, has the potential for use in monitoring crack development.

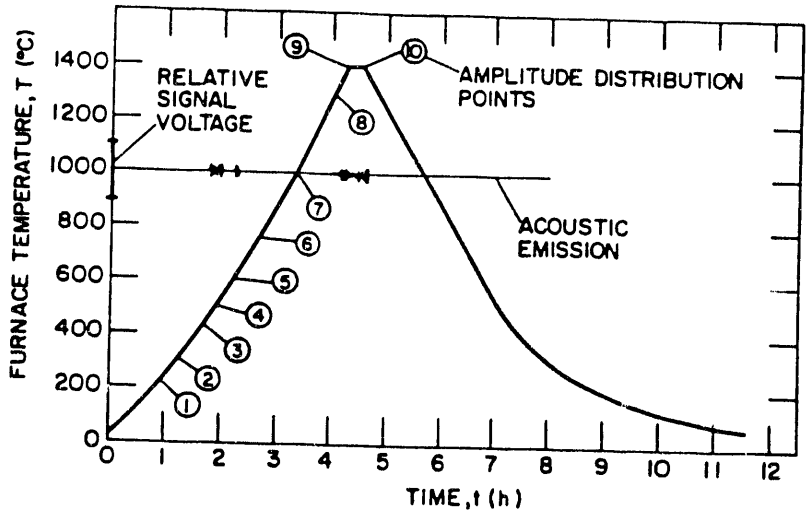

Fig. 22. Heat-up and cool-down temperature ramps used in test CT 220, and resulting location of acoustic activity

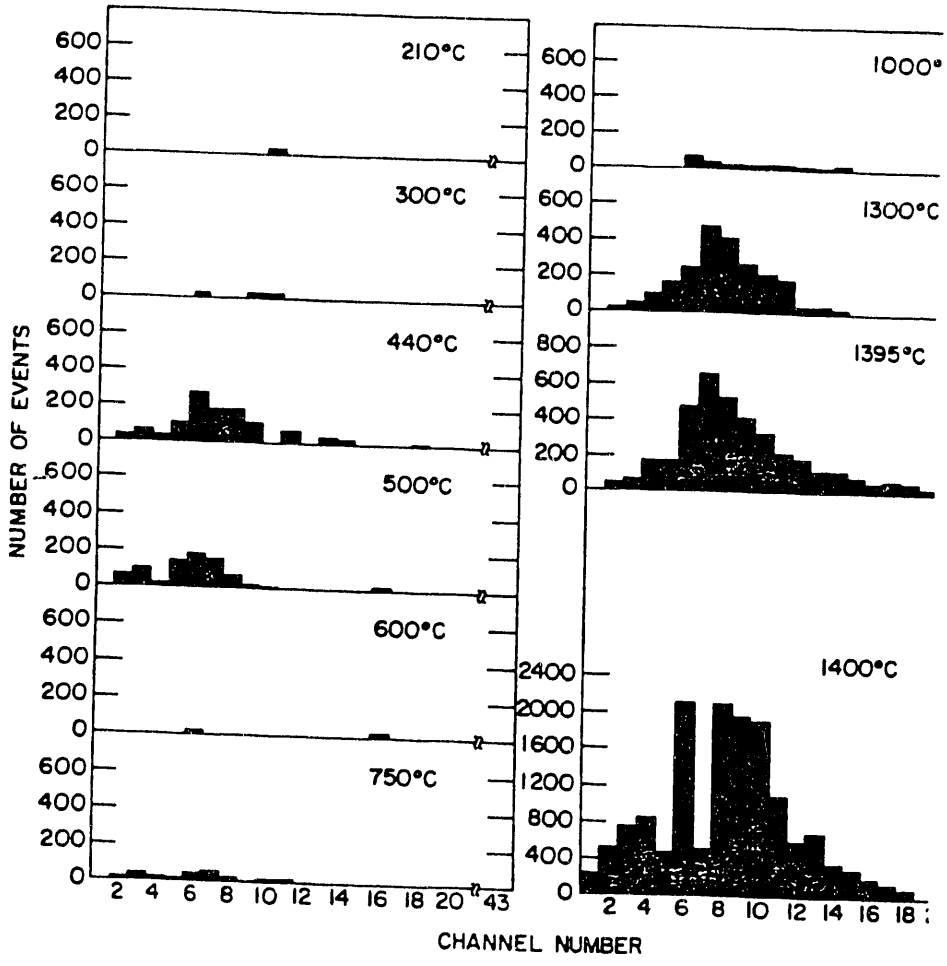

Fig. 23. Acoustic emission amplitude distribution of test CT 220

4 SUMMARY AND CONCLUSIONS

The fabrication process of the MSOFC has been reviewed from the standpoint of implementing a nondestructive characterization (NDC) program that would help ensure reliable manufacturing similar in many ways to that of ceramic capacitors.[32] The reviewed steps consisted of examining the starting materials, especially the special powders for the cathode and interconnect ($SrLaMnO_3$ and $LaCrO_3$, respectively); determining the critical organic additives used as binders, plasticizers, solvents, and poreformers; understanding details of blending powders and organics; studying the hot-roll calendering operation for single and trilayer tape production; understanding fuel and oxidant channel formation and possible defect formation; examining the debindering and sintering steps; and developing an understanding of the manifolding used to transport fuel and oxidants.

We have concluded that there is a significant role for NDC at each step in the production of MSOFCs. In powder characterization, the yttria-stabilized zirconia (YSZ) and NiO used for anode and electrolyte fabrication are available in high-commercial-grade powders. However, the $SrLaMnO_3$ and $LaCrO_3$ for the cathode and interconnector are limited in availability, and determination of their quality by extensive NDC would be appropriate. To date, it does not appear that anyone is using high-resolution microfocus X-ray imaging to sort powders for contaminants. This is becoming a widely used process for other ceramic processing areas and likely would be important here.

Although many different organics will likely still be investigated, the ability of these to blend uniformly is critical. The high sensitivity of ^1H NMR spectroscopy appears to offer an excellent method for characterizing the blended material. This will become especially important if salvage material will be combined with new material for cost reduction. Of possible concern is the effect of different thermal histories of each of the constituents of the blended materials when salvage material is added. Because no correlation seems to exist between rheological data and reliability of tapes, an effort appears warranted in this area.

We have also concluded that the area of highest priority for NDC is the as-calendered tapes. The single-layer tapes to be made into fuel channels are to be 305 μm thick. Because cracks in these tapes are of little importance except for loadbearing qualities, nondestructive characterization

here should focus mainly on uniformity of density to ensure uniformity of shape on firing. However, when the single-layer tapes are corrugated to form fuel/oxidant channels, significant residual stresses could be introduced and methods for measurement have been suggested. The trilayer tapes, on the other hand, are more critical. An A/E/C trilayer tape must be studied to determine density uniformity and the upper limit of porosity of the anode and cathode. However, the electrolyte should be examined closely for pores and possible cracks because it must be as tight as possible and of nearly 100% theoretical density. A combination of X-ray imaging methods (to detect voids or cracks), acoustic methods (for density uniformity), and infrared (for gross uniformity) seem to be implementable for this case.

When stack subassemblies are to be debindered and sintered, an NDC method seems almost mandatory for detection of cracking onset. This is important because the high weight percent of organic binders (≈30 wt.%), must be completely removed during debindering. Further, each of the organics (solvents, plasticizers, binders, and poreformers) will volatilize at a different temperature. During final sintering, control of heat-up and cool-down schedules must be critically maintained to avoid large temperature differences. This is especially true because of the differences in coefficients of thermal expansion, as well as of the possibilities of nonuniform organic content that will cause nonuniform shrinkage. It was concluded, for example, that anisotropy of residual stress levels may occur from the rolling direction. Methods of equilibrating these out (e.g., mild heat) may be helpful. Acoustic emission sensing methods with some form of signal analysis, e.g., histograms, energy measurement, etc., will be necessary. Following sintering, mounting of the manifold completes the stack assembly. Leakage rates of less than 0.1 vol.% for the H_2 fuel must be maintained, according to one design analysis. Leakage rates of the oxidant manifold should be less than 5 vol.%, according to the same design analysis. These are full-scale design values. When the entire assembly is completed, it is ready for testing.

It might be added that following sintering, and depending upon the acoustic emission activity detected, some form of inspection of each A/E/C or A/I/C should be made to check for through cracks. New high-quality optical borescopes may be implementable on an array basis.

5 RECOMMENDATIONS FOR FUTURE WORK

A summary of NDC suggestions is given in Table 5, along with a priority ranking. We suggest that the highest priority be given to development of NDC methods for as-calendered tapes, specifically the trilayer tapes. We suggest also that highest priority be given to development of acoustic emission to detect onset of cracking during sintering and to determine maximum outgassing of organics during debindering. Further, we suggest that high priority be given to development of NDC methods for as-calendered single-layer tapes and $SrLaMnO_3$ and $LaCrO_3$ powders. We suggest that development of NMR and FTIR spectroscopy be undertaken as NDC methods for as-blended material. This may require a higher priority should recyclable material be combined with new material. There is a concern about the impact of thermal histories and the molecular structure of the polymers.

Although not specifically noted here, if an organic bond material is used as an adhesive to bond A/E/C cells to interconnects, some form of NDC would be necessary to qualify these bonds. Sonic resonance methods have recently been developed for similar applications and we suggest this be pursued because of the relative inaccessibility of the surfaces for inspection.

ACKNOWLEDGMENTS

The author thanks the many people who kindly contributed to this report, including K. M. Myles, M. Krumpelt, R. B. Poeppel, U. Baluchandran, and A. C. Raptis. I also want to acknowledge the support of D. Moores, N. Heeg, and J. Fisher who helped in many ways to put this document together.

Clearly the sponsors, U.S. DOE/Fossil Energy/Morgantown Energy Technology Center, are to be acknowledged for their support.

Table 5. Summary of Possible NDC methods

Process Step (for material)	Starting Materials (powders) – $SrLaMnO_3$ $LaCrO_3$	Blended Materials	Flat As-Cast Green Tapes		Corrugated Green Tapes (formed channels)	De-bindering	Sintering	Non-manifolded Sintered Stack	Manifolded Sintered Stack
			Single Layer	Trilayer					
Defect Types; Material Character	Powder character-istics	Uniformity of blend, surface chemistry	Thickness density	Density, thickness, cracks	Residual stresses		Onset of cracking	Cracks in electrolyte or interconnect delamina-tions	Gas leakage
NDC Methods Suggested		^1H NMR spectroscopy	•Acoustic microscopy (two-sided) •Low-kV through-transmission X-ray •Infrared imaging		FTIR, Raman Spectro-scopy		Acoustic emission	Acoustic resonance, optical Holography, optical borescopes	Gas pressure by H_2 leak detection
Priority	High	Medium	Medium	Medium	Medium	High	Highest	Medium	Low

REFERENCES

1. Riley, B., "Solid-Oxide Fuel-Cells - The Next Stage," J. Power Sources, Vol. 29, pp. 223-237 (1990).

2. Trimble, K. A., "Solid-Oxide Fuel Cells," Gas Research Institute: Center for Advanced Materials, Vol. 4, No. 3, pp. 109-113 (1990).

3. Brown, J. T., "High-Temperature Solid-Oxide Fuel-Cells," Energy, Vol. 11, pp. 209-220 (1986).

4. Penner, S. S., "Assessment of Research Needs for Advanced Fuel Cells," U.S. Dept. of Energy Report DOE/ER-30060-TI (1985).

5. Prasad, V. C. S., and Kannan, P., "Comparison of Calendered and Tape-Cast Dielectrics," Am. Cer. Soc. Bull., Vol. 51, No. 11, pp. 1234-1235 (1982).

6. Schal, B. R., and Engel, H. J., "Calendering as a Method of Forming Thin Ceramic Sheets," Proc. Brit. Cer. Soc., Vol. 18, 281 (1970).

7. Hyatt, E. P., "Making Thin, Flat Ceramics -- A Review," Am. Cer. Soc. Bull., Vol. 65, No. 4, pp. 637-638 (1986).

8. Braun, L., Morris, J. R., and Cannon, W. R., "Viscosity of Tape-Casting Slips," Am. Cer. Soc. Bull., Vol. 64, No. 5, pp. 727-729 (1985).

9. Runk, R. B., and Andrejco, M. J., "A Precision Tape Casting Machine for Fabrication of Thin Ceramic Tapes," Am. Cer. Soc. Bull., Vol. 54, No. 2, pp. 199-200 (1975).

10. Mistler, R. E., "Tape Casting: The Basic Process for Meeting the Needs of the Electronics Industry," Am. Cer. Soc. Bull., Vol. 69, No. 6, pp. 1022-1026 (1990).

11. Natansohn, S., "Nondestructive Evaluation of Powders for Advanced Ceramics," in Proc. Nondestructive Testing of High-Performance Ceramics, Am. Cer. Soc., pp. 73-987 (1987).

12. Clark, D. R., and Adar, F., "Raman Microprobe Spectroscopy of Polyphase Ceramics," in Advances in Materials Characterization, Mat. Sci., Res. Vol. 15, D. R. Rossington, R. A. Condrate, and R. L. Synder, eds., Plenum Press, New York, pp. 199-214 (1982).

13. Carduner, K., Hatfield, G. R., Ellington, W. A., and Dieckman, S. L., "Nuclear Magnetic Resonance Spectroscopy and Imaging of High-Performance Ceramics," Handbook of Ceramics and Composites, Vol. 2, W. P. Cheremisinoff, ed., Marcel-Deila, New York, pp. 965-501 (1992).

14. National Materials Advisory Board, "Automated Nondestructive Characterization and Evaluation in Metal and Ceramic Powder Production," U.S. Army Materials Technology Laboratory Report MTL-TR/86-34 (1986).

15. Friant, C. L., "Ultrasonic Nondestructive Characterization Approaches for Structural Ceramics," in Proc. 21st SAMPE Technical Conf., Vol. 21, pp. 1067-1076 (1989).

16. Guyott, C. C. H., and Cawley, P., "Evaluation of Cohesive Properties of Adhesive Joints Using Ultrasonic Spectroscopy," NDT International, Vol. 21, No. 4, pp. 233-240 (1988).

17. Kupperman, D. J., and Karplus, H. B., "Ultrasonic Wave Propagation Characteristics of Green Ceramics," Am. Cer. Soc. Bull. Vol. 63, No. 12, pp. 1505-1509 (1989).

18. Lynworth, L. C., Papadakais, E. L. and Rea, W. R., "Ultrasonic Measurement of Phase and Group Velocities Using Continuous Wave Transmission Techniques," Proc. IEEE Symp. on Ultrasonics, pp. 533-536 (1973).

19. Sachse, W., and Pao, Y. H., "On The Determination of Phase and Group Velocities of Dispersive Waves in Solids," J. of Appl. Phys., **49**, 4320-4327 (1978).

20. Brekhovskikh, L. M., "Waves in Layered Media," 2nd Ed., Academic Press, New York, pp. 370-371 (1980).

21. Zhu, Y. M., Babit, D., and Peix, G., "A Quantitative Comparison between Linear X-ray Sensitive Array and Image-Intensifier Systems," NDT International, Vol. 23, No. 4, pp. 214-220 (1990).

22. Wenk, S. A., "Real-Time Radiography," Proc. World Conf. on NDT, Vol. 1, pp. 536-552 (1985).

23. Friedman, W. D., Harris, R. D., Engles, P., Hunt, P. K., and Srinivasan, M., "Characterization of Green Ceramics with X-ray Tomography and Ultrasonics," Proc. Conf. on Nondestructive Testing of High-Performance Ceramics, Boston, Aug. 25–27, pp. 128–131 (1987).

24. Roth, D. J., Stang, D. B., Swickard, S. M., DeGuive, M. R., and Dolhert, L. E., "Review, Modeling, and Statistical Analysis of Ultrasonic Velocity -- Pore Fraction Relations in Polycrystalline Materials," Mat. Eval., pp. 883-888 (July 1991).

25. Mendoza, E. A., and Cannon, W. R., "Measurement of Residual Stresses Using FTT Rand Raman Microprobes", Proc. Conf. on Nondestructive Evaluation of Modern Ceramics, July 9–12, 1990, Columbus, OH, pp. 106–110.

26. Ellingson, W. A., "Nondestructive Evaluation for Monolithic Fuel Cells," in Monolithic Fuel Cell Development Quarterly Status Report, Nov. 1984-Jan. 1985, Argonne National Laboratory, pp. 10-38 through 10-47 (Feb. 7, 1985).

27. Ellingson, W. A., "Nondestructive Evaluation for Monolithic Fuel Cells," in Monolithic Fuel Cell Development Quarterly Status Report, June-August 1985, pp. 10-26 through 10-42 (Oct. 11, 1985).

28. Reynolds, W. N., "Inspection of Laminates and Adhesive Bonds by Pulse-Video Thermography," NDT International, pp. 229-232 (Aug. 1988).

29. Halmshaw, R., "Nondestructive Testing," Edward Arnold publishers, Victoria, Australia.

30. Vavilor, V. P., and Taylor, R., "Theoretical and Practical Aspects of the Thermal Nondestructive Testing of Bonded Structures," in Research

Techniques in Nondestructive Testing, Vol. V, R. S. Sharpe, ed., pp. 239-279 (1982).

31. Majumdar, S., Claar, T., and Flandermeyer, B., "Stress and Fracture Behavior of Monolithic Fuel Cell Tapes," J. Am. Cer. Soc., Vol. 69, No. 8, pp. 628-633 (1986).

32. Ewell, G. J., "Multi-layer Ceramic Capacitors; Review of Nondestructive Testing Methods," Internal Report, Hughes Aircraft Co., Culver City, CA, (Oct. 1981).

Distribution for ANL–92/24

Internal:

S. Ahmed
J. G. Asbury
J. E. Battles
I. D. Bloom
D. W. Dees
H. Drucker
W. A. Ellingson (10)
M. Krumpelt (5)
G. H. Kucera
R. Kumar
C. A. Malefyt
K. M. Myles
R. B. Poeppel
A. C. Raptis
W. J. Shack
C. E. Till
R. A. Valentin
R. W. Weeks
D. J. Zurawski
ANL Patent File
TIS Files

External:

DOE–OSTI, for distribution per UC–110 (42)
D. T. Goldman, DOE–CH
F. Herbaty, DOE–CH
J. Jonkowski, DOE–CH
ANL Libraries
ANL–E
ANL–W
Manager, Chicago Field Office, DOE
MCT Division Review Committee:
H. K. Birnbaum, U. of Illinois at Urbana–Champaign, Urbana
R. C. Buchanan, U. of Cincinnati, Cincinnati
M. S. Dresselhaus, Massachusetts Inst. of Technology, Cambridge
B. G. Jones, U. of Illinois at Urbana–Champaign, Urbana
C.–Y. Li, Cornell U., Ithaca, NY
S.–N. Liu, Electric Power Research Inst., Palo Alto, CA
R. E. Smith, Engineering Applied Sciences, Inc., Trafford, PA

ABB–COMBUSTION ENGINEERING, P. Kantesaria, Windsor, CT
ALLISON GAS TURBINE DIVISION, H. F. Creveling, Indianapolis, IN
ARINC RESEARCH CORPORATION, D. M. Berkey, Annapolis, MD
ARTHUR D. LITTLE, INC., P. Teagan, Cambridge, MA
BABCOCK & WILCOX, E. A. Barringer, Lynchburg, VA
BECHTEL CORPORATION, J. R. Bowden, San Francisco, CA
BP AMERICA, T. L. Cable, Cleveland, OH
CATERPILLAR, INC., TECHNICAL CTR. – A, T. J. Richards, Peoria, IL
CENTER FOR ELECTROCHEMICAL SYSTEMS & HYDROGEN RESEARCH (CESHR), J. A. Appleby, College Station, TX
CERAMATEC, INC., C. E. Milliken, Salt Lake City, UT
DARPA, R. L. Rosenfeld, W. Coblenz, Arlington, VA
DETROIT DIESEL CORPORATION, T. D. Laymac, Detroit, MI
DOW CHEMICAL USA, G. A. Eisman, Midland, MI
EG&G IDAHO, INC., P. A. Lessing, Idaho Falls, ID
ELECTRIC POWER RESEARCH INSTITUTE, E. A. Gillis, Palo Alto, CA

ENERGY RESEARCH CORPORATION, H. C. Maru, Danbury, CT
EXXON, P. Grimes, Linden, NJ
FLORIDA POWER & LIGHT COMPANY, R. S. Allen, West Palm Beach, FL
FMC CORPORATION, G. E. Foltz, Bessemer City, NC
GAS RESEARCH INSTITUTE, M. P. Whelan, Chicago, IL
GENERAL MOTORS, C. Huang, Warren, MI
GENERAL MOTORS, C. E. Miller, Flint, MI
GENERAL MOTORS – A.C. ROCHESTER DIVISION, R. S. Taylor, Flint, MI
GILBERT/COMMONWEALTH, INC., J. H. Hirschenhofer, Reading, PA
IIT RESEARCH INSTITUTE, C. R. Unkle, Rome, NY
INTERNATIONAL FUEL CELLS CORPORATION, J. S. Caraceni, So. Windsor, CT
INSTITUTE OF GAS TECHNOLOGY, R. J. Remick, Chicago, IL
LAWRENCE BERKELEY LABORATORY, K. Kinoshita, Berkeley, CA
M-C POWER CORPORATION, E. H. Camara, Burr Ridge, IL
NASA LERC GROUP, T. M. Maloney, Brook Park, OH
NASA LEWIS RESEARCH CENTER, P. Prokopius, Cleveland, OH
NEW YORK POWER AUTHORITY, P. M. Winegar, New York, NY
PACIFIC ENERGY, M. H. Clinton, Commerce, CA
PACIFIC NORTHWEST LABORATORY, J. L. Bates, Richland, WA
ROLLS-ROYCE, INC., J. Wills, Washington, DC
SANDIA NATIONAL LABORATORIES, N. Doddapaneni, Albuquerque, NM
SCIENCE APPLICATIONS INTERNATIONAL CORP., J. E. Cassady, Seattle, WA
SOUTHERN CALIFORNIA EDISON, R. H. Sliwoski, Rosemead, CA
SOUTHERN CALIFORNIA EDISON, N. W. Patapoff, Jr., Irwindale, CA
SRI INTERNATIONAL, B. G. Pound, Menlo Park, CA
TEXAS A&M UNIVERSITY, A. J. Appleby, College Station, TX
US DEPARTMENT OF ENERGY, E. F. Beyma, Washington, DC
US NAVY, DAVID TAYLOR RESEARCH CENTER, M. C. Cervi, Annapolis, MD
US NAVY, NAVAL UNDERWATER SYSTEMS CENTER, P. M. Dunn, Newport, RI
UNIVERSITY OF MINNESOTA, D. A. Shores, Minneapolis, MN
UNIVERSITY OF MISSOURI-ROLLA, H. U. Anderson, Rolla, MO
UNOCAL, M. H. Ghandehari, Brea, CA
VIRGINIA ELECTRIC & POWER COMPANY, G. A. Verno, Glen Allen, VA
WESTINGHOUSE ELECTRIC CORPORATION, W. J. Dollard, W. A. Summers,
L. E. Van Bibber, S. E. Veyo, Pittsburgh, PA
ZTEK CORPORATION, M. S. Hsu, Waltham, MA

DATE
FILMED
8/10/93
END